Master's Thesis

Utrecht University

Faculty of Geosciences
Department of Physical Geography
Earth Surface and Water

Modelling and quantifying runoff and soil loss for a degraded and restored Jordan side wadi

Author:
Emily Gotink

Supervisors:
Prof. dr. Steven de Jong
Dr. Stefan Strohmeier

June 30, 2022

Final version

Abstract

Water erosion is the most widespread land degrading process worldwide. Especially in drylands, this process is intensified by anthropogenic pressure on soil productivity, resulting in a self-reinforcing effect of topsoil removal, declining vegetation and increased runoff generation. This process is also ongoing in Jordan, where recurring droughts, years of overgrazing and mismanagement of agricultural land has led to removal of native vegetation and consequential land degradation through water erosion. Steep slopes of the side wadis that border the Jordan Valley exacerbate these problems, causing flash floods and clogging of water collection ponds. A SIDA-FAO-funded project of The International Centre for Agricultural Research in Dry Areas (ICARDA) arose to test rehabilitation implementation on small scale and thereby increase local stakeholders' preparedness for uptake and out-scaling. Therefore, this research aimed to study and quantify surface runoff and soil loss in a Jordan side wadi during its degraded state and after modelled implementation of restoration measures. Simultaneously, erosion hotspots and restoration potential were identified for targeted erosion control. A hydrological pre-assessment was performed for model validation, using the curve number approach, runoff ratios and erosion feature field analyses. An erodibility map was created in GIS based on literature, datasets and field validation. Representative hotspots were selected for additional fieldwork to collect input for the Rangeland Hydrology and Erosion Model (RHEM). This process-based hillslope model was chosen for runoff and soil loss quantification as it has proven to be successful for the Jordan rangelands. It requires rainfall data, soil texture, slope- and cover characteristics. The CLimate GENeration model (CLIGEN) was bias corrected with a local rainfall data, resulting in a 300-year simulation of rainfall statistics. Soil texture and cover characteristics were collected through fieldwork at the hotspot classes and a stream network assessment was performed to obtain representative slope-length combinations, which were used to upscale from hillslope- to wadi level. The degraded scenarios yielded a runoff ratio of 10,7%, which was in agreement with the hydrological pre-assessment. Soil loss was estimated to be 2,31 ton/ha/y, with maximum hotspots of 4,99 ton/ha/y. This was lower than expected, which could likely be attributed to high rock content at the fieldwork sites. Restored equilibrium scenarios yielded an average reduction of 21,8% in runoff and 53,4% in soil loss for the entire wadi, emphasizing the impact of increased vegetation cover on the ecosystem's resilience. Direct impact of intended WH structures was assessed by a script based on pit dimensions, infiltration rate and trapping efficiency. Runoff process description of the script lacked detail, underestimating runoff capturing capacity and overestimating sediment buffer capacity, yet providing a rough tool for determining optimal pit dimensions and spacing. This yielded an average decrease of 35% in runoff and 71% in soil loss for the restorable scenarios.

Keywords: Drylands, Land degradation, Jordan side wadis, RHEM, Surface runoff, Water erosion, Water harvesting, Watershed rehabilitation

Contents

List of Figures

List of Tables

Acronyms

AMC	Antecedent Moisture Condition.
ARS	Agricultural Research Service.
CLIGEN	CLimate GENeration model.
CN	NRCS Runoff curve number.
DEM	digital elevation model.
FAO	Food and Agriculture Organization of the United Nations.
GDS	Graphic Data System.
GE	Google Earth Pro.
GIS	ArcGIS Pro.
HRU	Hydrologic Response Units.
HSG	Hydrologic Soil Groups.
ICARDA	The International Centre for Agricultural Research in Dry Areas.
KINEROS2	Kinematic Runoff and Erosion Model.
LJRB	Lower Jordan River basin.
MWI	Ministry of Water and Irrigation.
NOAA	National Oceanic and Atmospheric Administration.
NRCS	Natural Resources Conservation Service.
RCC	runoff capturing capacity.
RHEM	Rangeland Hydrology and Erosion Model.
RMSE	Root Mean Squared Error.
SCC	sediment capturing capacity.
SIDA	Swedish International Development Cooperation Agency.
SLC	slope-length combination.
TE	trapping efficiency.

USDA United States Department of Agriculture.

WH water harvesting.

Chapter 1

Introduction

1.1 Background

1.1.1 Drylands and desertification across the world

Drylands are regions that are characterized by low water availability and consist of dry sub-humid, semi-arid, arid and hyper-arid regions. These critical terrestrial systems occupy as much as 45% of the global land area. They are prone to environmental issues such as land degradation, which can even lead to desertification. The definition of desertification is land degradation in dry sub-humid, semi-arid and arid regions which can result from either natural and/or anthropogenic factors (Prăvălie, 2016; Veron et al., 2006). It can lead to a substantial reduction in ecosystem services (Dregne and Chou, 1992).

In most parts of the world the easily developed land is already exploited. With a rapidly increasing world population and thus an increasing need for agricultural land, people are forced to turn to more arid regions. This increased pressure on the drylands enhances water stress and land degradation. Thus, effective land- and water management is key and it requires good understanding of the hydrological processes in these dry regions (Sen, 2008; Wheater and Al Weshah, 2002).

1.1.2 Water erosion

Worldwide, water erosion is the most widespread land degrading process. Water erosion is the detachment, transport and deposition of soil particles and thus a soil loss inciting process. This process is aggravated by anthropogenic factors such as the agricultural pressure in drylands, which has a negative impact on crop productivity, soil resources and environmental quality (Ravi et al., 2010; Lal et al., 1994). Water erosion is an event-based process which can be spatially restricted by topography and land use conditions. Other dominant factors at play are rainfall intensity, slope and antecedent soil moisture content (Ziadat and Taimeh, 2013; Breshears et al., 2003).

The two requirements for water erosion are rainfall and runoff production. Raindrops of sufficient kinetic energy will detach soil particles at impact which is also known as splash erosion. Indirectly, the runoff produced by rainfall can detach and transport the soil particles through sheet-, rill- and (ephemeral) gully erosion (Figure 1.1). This results in the removal of nutrient-rich topsoil which affects the establishment and survival of vegetation. Less vegetation means less roots to promote

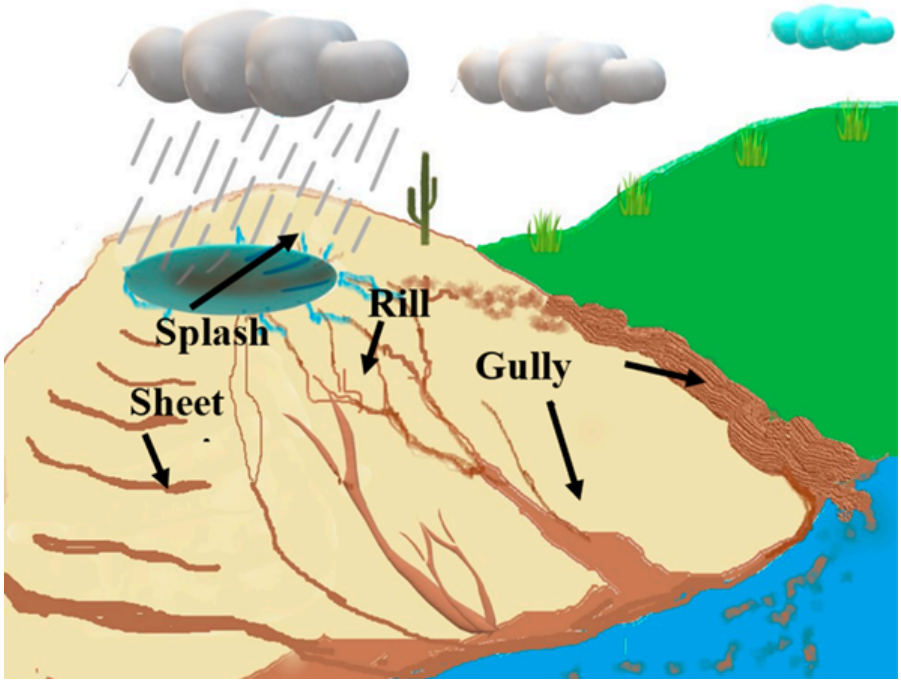

Figure 1.1: Types of water erosion. Adopted from: Senanayake et al. (2020)

soil stability and a decrease in infiltration capacity. These are conditions that promote runoff erosion even more: a positive feedback (Ravi et al., 2010; Lal et al., 1994). Especially in drylands, dry and bare soils in combination with high intensity storm events can generate large amounts of runoff and soil erosion in a short amount of time (Farhan et al., 2016).

1.1.3 Modelling of runoff and soil loss

The complexity of processes that drives and determines quantities of runoff and soil erosion result in various modelling approaches. Since the 1940's scientists have been developing these conceptual, empirical or process/physically-based models (Figure 1.2) in order to quantify runoff and soil loss for approximately 32% of the Earth's land surface Borrelli et al. (2021). Out of these, physically-based models are best at simulating real hydrologic responses as they incorporate physical laws and equations. This allows for detailed simulation of spatial and temporal variability, which could be considered its strength and simultaneously its weakness: they might require extensive input and site specific calibration (Sitterson et al., 2018). Modelling approaches can either be of small (hillslope or plot) scale, such as the Rangeland Hydrology and Erosion Model (RHEM) or large (watershed) scale, such as the Kinematic Runoff and Erosion Model (KINEROS2). Due to its scale, specifically the latter often requires extensive input parameters for proper simulation, while the RHEM only requires soil texture, slope- and cover- characteristics. Additionally, validation is considered difficult and lacking on watershed scale, which poses limits to watershed scale models. Especially validation through field data is often unavailable (Govers, 2011). Nonetheless, this spatial scale is chosen most

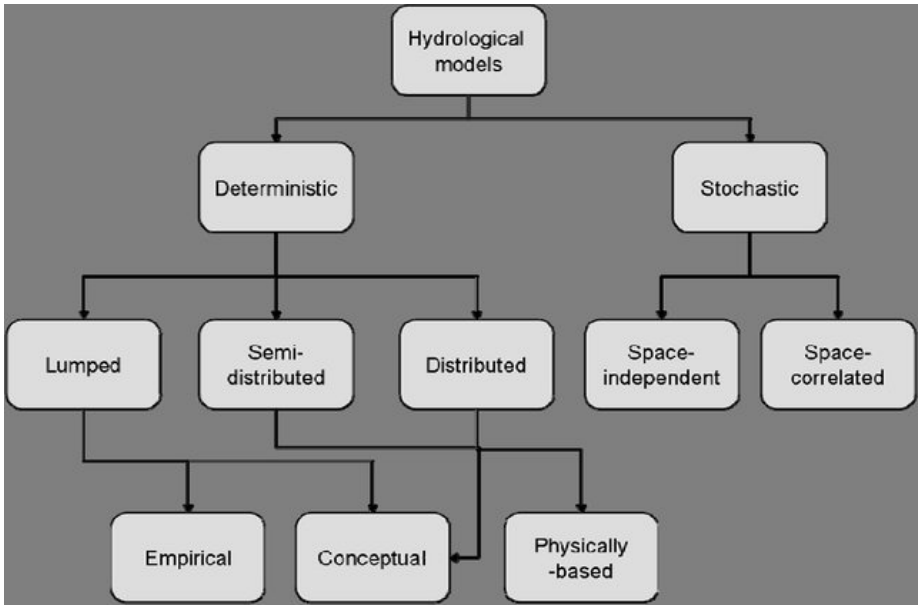

Figure 1.2: General classification of hydrological models. Adopted from Chow et al. (2005)

often in modelling applications (Alewell et al., 2019; Auerswald et al., 2003; Borrelli et al., 2021; De Vente et al., 2013; De Vente and Poesen, 2005).

1.2 Problem definition

Jordan is one of the places where soil erosion by water is an increasing problem Food et al. (1979); Farhan et al. (2013). Recurring droughts and years of overgrazing and mismanagement of agricultural land has led to the removal of native vegetation cover and consequential degradation through rainfall and surface runoff. Especially near the Jordan Valley, which is bordered to the east by steep escarpments. A greater relief is associated with large amounts of soil erosion (Zhang et al., 2013). During the rainy season, the side wadis at these slopes become prone to water erosion. Erosion of the topsoil leads to a further decline of the soil productivity, which is enhanced by the increased need for fertile land due to population growth (Khresat, 2013). In addition, the degraded side wadis show an increased risk of flash flood events during rainstorms and were classified as 'high risk' regarding flood hazard (AlMahasneh et al., 2021). The dry and crusted soil results in poor infiltration of rainwater, increasing runoff and soil erosion, which leads to an even further decline in potential fertile soil (Farhan et al., 2013). Simultaneously, these relatively undocumented regions attribute to problems downstream in the Jordan Valley, which is considered the agricultural heart of Jordan. The most significant one is the clogging of water collection ponds used for irrigation and water storage.

The International Centre for Agricultural Research in Dry Areas (ICARDA) has projects that target the restoration of the Jordan rangelands by restoration measures that increase the amount of vegetation and capture runoff, to eventually boost agricultural productivity. These measures

are executed through various strategies. One is soil and water conservation (SWC), to enhance land productivity adapted to a local soil-, water- and vegetation circumstances in degraded areas. Another strategy is sustainable land management (SLM), which focuses on the use of land resources while ensuring sustainability. These strategies prosper from collaboration with and feedback from local community, since sustainable management is required after implementation of measures. On of these measures is planting scrubs and trees in mechanized and manual water harvesting (WH) structures. These WH structures have proven to be successful in decreasing soil loss and runoff in the Jordan rangelands (Strohmeier et al., 2021). So far, the WH structures have only been implemented and tested in the arid Badia of Jordan. The question arises whether those structures would have the same desired effect in the side wadis along the Jordan Valley. Potentially, the side wadis could be treated with similar WH structures. Capturing water and soil upstream could increase productivity and livelihood upstream, yet capturing too much runoff would deplete the downstream irrigated agriculture of the Jordan Valley. Is is therefore important to study the local impact that these measures would have on surface runoff and sediment transport is currently unknown. This has developed into a new project of ICARDA, funded by the Food and Agriculture Organization of the United Nations (FAO) and the Swedish International Development Cooperation Agency (SIDA), on studying these effects. The project, which was called: 'Planning and piloting watershed rehabilitation for improved water productivity with water-harvesting in Jordan' desires this study to determine whether large scale implementation has potential and to increase local stakeholders' preparedness for uptake and out-scaling by emphasizing the potential positive effects (SIDA-FAO)(project link).

Erosion simulation models are important tools in quantifying current and future water erosion in the side wadis and watersheds in general. Especially hillslope models, since hillslopes surfaces are the zones in watersheds which are especially prone to water erosion (Santhi et al., 2006; He, 2003; Lu et al., 2006; Miller et al., 2007). The Rangeland Hydrology and Erosion Model (RHEM) is such process-based erosion model that simulates runoff and soil loss on a hillslope scale. Its input parameter demand is manageable and collectable via fieldwork. It models the soil loss, sediment yield and runoff response for a single rain storm for single events up to 300 year simulations (Felegari et al., 2014). The model has proven to be successful for the Jordan rangelands, and it allows to simulate various vegetation scenarios that can assess the impact of restoration measures (Strohmeier, 2017). Therefore, this study will use the RHEM model to quantify, validate and upscale runoff and soil loss for a Jordan side wadi before and after implementation of potential restoration measures.

1.3 Aim and objectives

The aim of this research is to study and quantify surface runoff and soil loss by water erosion for an entire Jordan side wadi (23 km^2) during its current degraded state and after modelled implementation of restoration measures. Subsequently, this makes it possible to assess whether large-scale implementation of restoration measures by the SIDA-FAO project would have the desired effect of reaching a sustainable ecosystem, where there is balance between water erosion and the ecosystem's resilience, as well as enhancing rangeland agricultural productivity. Simultaneously, it serves as an analysis to identify erosion hotspots and potential restorable areas in the wadi. Emphasizing the potential effects of wadi restoration should eventually increase local stakeholders' preparedness for uptake and out-scaling.
This leads to the following objectives:

I. Hydrological pre-assessment of a selected side wadi for model validation.

II. Mapping of erosion hotspots and restorable areas for targeted future erosion control.

III. Quantification of runoff and soil loss values in the wadi using RHEM for various scenarios;

   a. The current degraded phase

   b. The restored equilibrium phase

   c. The WH phase: a direct impact assessment of WH structures on runoff and soil loss in the degraded wadi.

Chapter 2

Study area

2.1 Lower Jordan Valley basin

The Jordan River basin is a 223 km long, north-south-oriented, transboundary river basin hosting the Jordan River. The Jordan River originates from the Anti-Lebanon- and Mount Hermon mountain ranges and discharges into the Dead Sea. The basin is 18,285 km^2 and its five riparian countries are: Lebanon, Syria, Israel, Palestine and Jordan (Comair et al., 2012). The geographical region of the basin that is situated within the Jordan country borders is called the Lower Jordan

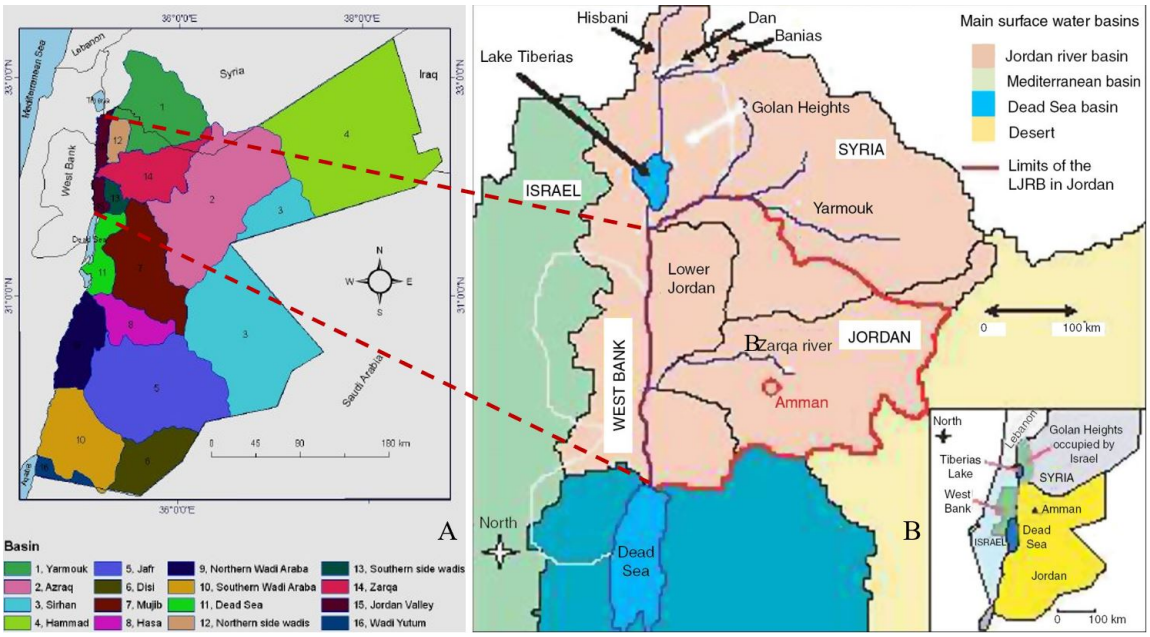

Figure 2.1: A: Sub-basins of the LJRB, B: Geographical extent of the LJRB. Adopted from, respectively, Al-Ansari et al. (2014) and Venot et al. (2008).

River basin (LJRB) (Figure 2.1B). This basin is subdivided into Yarmouk-, Zarqa-, Jordan Valley-, Southern side wadis- and Northern side wadis basin (Figure 2.1A).

To the east, the Jordan Valley basin is bordered by steep slopes that are incised by the side wadis of the so called Northern- and Southern side wadis basin. These wadis are bounded by steep banks and characterized by ephemeral streams. During the rainy season these valleys become westerly flowing watercourses. In arid regions such as Jordan, the words 'wadi' and 'watershed' are often used intertwined. By definition, wadis and watersheds mainly differ in humidity, hence the ephemeral flow. When the ratio of annual precipitation and potential evapotranspiration $\frac{P}{PET}$ is smaller than 0.2, the region is classified as arid to hyper arid. A ratio between 0.2-0.5 indicates semi-arid conditions and a ratio between 0.5-1 indicates a sub-humid to humid region (Barrow, 1992).

2.2 Selected fieldwork site

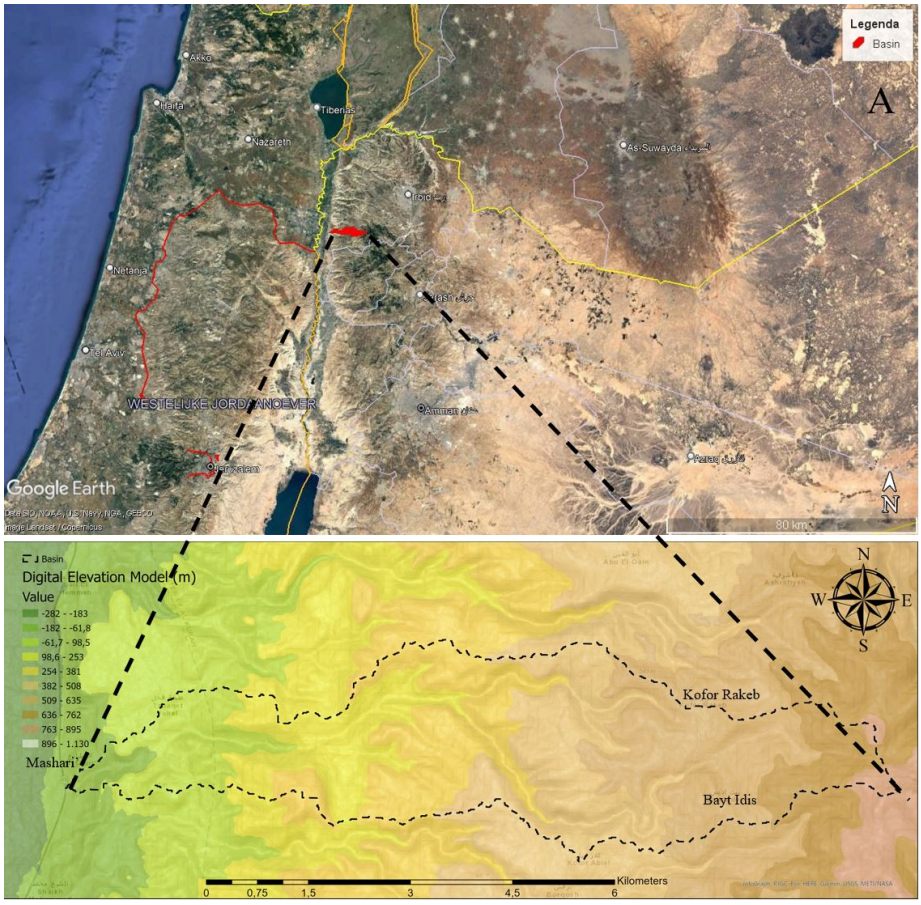

Figure 2.2: A: Geographical- (A) and exact (B) perspective of the selected fieldwork site.

For this study the suitability of the wadi depended on its spatial extent and -characteristics, and on the availability of required data for modelling and validation purposes. In order to allow an optimal field measurement coverage, a relatively small sized wadi was preferred. A minimized upstream area ensures little interference of unknown sources of sediments and runoff. In terms of efficiency, a wadi in the proximity of inhabited areas was favored as it increased the accessibility of the fieldwork site. In addition, this allows for narrative and semi-quantitative data and feedback from local communities during local erosion assessments and future restoration activities. An ALOS PALSAR digital elevation model (DEM) of 2009 (ALOS-PALSAR, 2009) with a spatial resolution of 12,5 m was utilized. With the use of ArcGIS pro (Esri-Inc., 2021) the DEM was used to delineate the watersheds in the LJRB, so that their physical extent and characteristics could be determined.

The chosen study area is located in the Northern side wadis basin, roughly in between the villages Mashari' and Bayt Idis of the Irbid Governorate (Figure 2.2). The basin is east-west oriented and covers an area of approximately 21 km^2. It has an approximate length and width of respectively 15 km and 1,5 km. The highest point of the watershed is 900 m above sea level and the lowest point is 260 m below sea level: an elevation difference of 1160 m between the upper part of the watershed and the outflow point. The effect of this strong altitude gradient on precipitation becomes clear as average annual rainfall ranges between 350 in the west to 500 mm in the east. This falls mostly in the rainy season between November and April (Al-Omari et al., 2015). A Mediterranean semi-arid climate prevails with a highest mean temperature of 27 °C in August and a lowest mean temperature of 10 °C in January (WorldBank, 2021). The major part of the wadi consists of grassland and bare land, and the soil texture ranges from clay loam to silty clay loam (ESA-Worldcover, 2020; Rawajfih et al., 1987; ISRIC, 2017).

Chapter 3

Methodology

3.1 The Rangeland Hydrology and Erosion Model

The Rangeland Hydrology and Erosion Model (RHEM) was chosen for quantification of runoff and soil loss amounts at the side wadis. The first version of the model was developed in 2006 by the United States Department of Agriculture-Agricultural Research Service (USDA-ARS). It used physically-based hydrologic- and erosion concepts from the Water Erosion Prediction Project (WEPP), whose equations were based on cropland data. These equations were modified for the application of rangelands (Nearing et al., 2011; Flanagan and Nearing, 1995). Over the years, the RHEM was adapted and improved multiple times to optimally capture and model the complex interactions between soil properties, land- and ground cover and hydrologic- and erosion processes.

The major improvements include implementation of stream power which makes it possible to simulate sediment transport of concentrated flow erosion (Al-Hamdan et al., 2012), a newly developed splash- and sheet equation (Al-Hamdan et al., 2017) and a sediment continuity equation that is based on the kinematic wave routing and runoff, which was derived from the KINEROS2 model (Hernandez et al., 2017; Goodrich et al., 2012; Woolhiser et al., 1990). For infiltration rate the RHEM uses the three-parameter equation, which is the combination of the models of Green and Ampt (1911) and Smith and Parlange (1978), which comprise two parameters for soil characterisation, saturated hydraulic conductivity and capillary forces, and one variable to characterize the initial soil moisture condition. A description of the main equations of overland flow, soil erosion, transport and deposition can be found in Hernandez et al. (2017) and the equations are attached in Appendix A.

Additionally, the latest version of the RHEM comprises a web-based and accessible interface where scenarios can be constructed, run and compared based on specified rainfall station data (RHEM Web Tool). It uses the stochastic CLimate GENeration model (CLIGEN) to produce daily rainfall statistics for a 300 year period based on historic measurements from one of the chosen stations that are embedded in RHEM (Hernandez et al., 2017). Since 2003 it is also possible to manually create a CLIGEN station file. This allows users to use the statistical characteristics of their own rainfall station data for synthetic time series generation of weather data with CLIGEN. First, the data needs to be formatted in one that is accepted by the "GenStPar.exe" function. This file is called the Graphic Data System (GDS) file, which can be created with a python script (Appendix B.1) (Nouwakpo, 2022a). Next, the "GenStPar.exe" program builds the .TOP file. This

file contains the headers of the GDS file and the monthly averages and standard deviations from the proposed data record. Thereafter the "FindMatch.exe" program uses the .TOP file to search for a surrogate station and generate the CLIGEN station. The surrogate station is one of the fully instrumented and documented U.S. stations which are supplied by RHEM. The algorithm uses a least squares statistic on monthly transition probability P(W—W) (wet to wet day), P(W—D) (dry to wet day), elevation and latitude with weights of respectively 49%, 49%, 1% and 1% (Yaoming et al., 2004). This way a surrogate station with data resembling the proposed data record best is chosen to provide additional information which regular stations lack. Executables can be found online (CLIGEN executables). Finally, the generated CLIGEN station file needs some editing by means of a python script (Appendix B.2) (Meyer, 2011; Nouwakpo, 2022b). This script edits the order of columns to a format that is expected by RHEM.

In terms of rangeland application, an important aspect of the RHEM is its inclusion of plant growth forms and surface ground cover data in the parameterization of the RHEM under 'cover characteristics' (Hernandez et al., 2017; Nearing et al., 2011). Foliar cover is distinguished as bunch grass, forbs/annual grass, shrubs and sod grass. This type of cover is highly susceptible to seasonal or climatic fluctuations. Ground cover is less susceptible to these fluctuations, and is distinguished in basal plant cover, rock cover, litter cover and biological crust cover. Both covers intercept and dissipate the kinetic energy of rainfall. Additionally, ground cover slows down runoff and protects the soil from eroding. The remaining input parameters (Figure 3.1) are slope shape and steepness, soil texture class of the top 4 cm and rainfall data. The output report consists of the annual average runoff and erosion rates and the return period of runoff and erosion rates. This extensive parameterization and highly process-based nature of the RHEM makes that local calibration is not compulsory (Haddad et al., 2022).

3.2 Pre-diagnostics of a suitable wadi

3.2.1 Data availability

The wadi was selected by means of watershed delineation and based on spatial criteria as described in section 2.2. Watershed delineation was done using a high resolution DEM (12,5 m) and the Watershed Tool procedure of GIS. The Jordan Ministry of Water and Irrigation (MWI) was approached for daily in-situ rainfall and runoff data in the proximity of the fieldwork site. These stations are shown in figure 3.2. Rainfall data from either the centre or the outer east and west of the wadi was favoured because the wadi crosses an annual rainfall range from 350 mm to 500 mm (Figure 3.3). As temporal data coverage of the western station appeared insufficient, the decision was made to proceed with the eastern situated station of Kufr Awan. The archive of this station consists of daily measurements ranging from the year 1981 to 2020. The runoff station of Wadi Ziglab was selected to validate runoff modelling, but was discarded in the process as there was a poor relation with the rainfall data of Kufr Awan (Appendix C). Instead, runoff ratios were retrieved for the Jordan Valley basin and for the North- and South side wadi basin.

3.2.2 Quick runoff and soil loss assessment

A quick hydrological assessment was performed to obtain a first impression about the runoff volumes and the erosion quantities in the wadi. Simultaneously, these values were used to compare with RHEM modelling output.

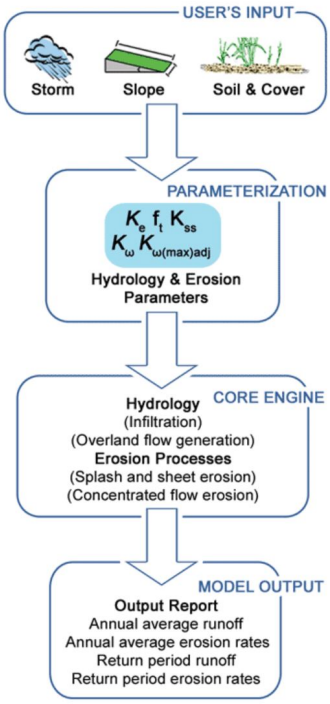

Figure 3.1: Flowchart of the RHEM prediction procedure. Adopted from `https://apps.tucson.ars.ag.gov/rhem/about`

Curve number

The NRCS Runoff curve number (CN) assessment was implemented to calculate surface runoff for the wadi and validate runoff quantities from RHEM (USDA, 1986). Additionally, the calculated CN was included as erosivity factor in the erosion hotspot map that was created. The CN is a method for estimating runoff (Q, mm) after a rainfall event (P, mm) according to equation 3.1:

$$Q = \frac{(P - 0.2S)^2}{P + 0.8S} \text{ if } P > 0.2S \quad \text{and} \quad Q = 0 \text{ if } P < 0.2S \tag{3.1}$$

Where S is the storage (equation 3.2), which is a varying parameter that is based on the CN as follows:

$$S = \frac{25400}{CN} - 254 \tag{3.2}$$

The CN value is based mainly on land use and Hydrologic Soil Groups (HSG) of the area of interest (Huang et al., 2007). The HSG account for the variety of different soil types' ability to infiltrate and are defined by the United States Department of Agriculture (USDA)-Natural Resources Conservation Service (NRCS). The groups range from A to D indicating, respectively, high to very low infiltration capacity. The soil moisture condition before runoff occurs is another

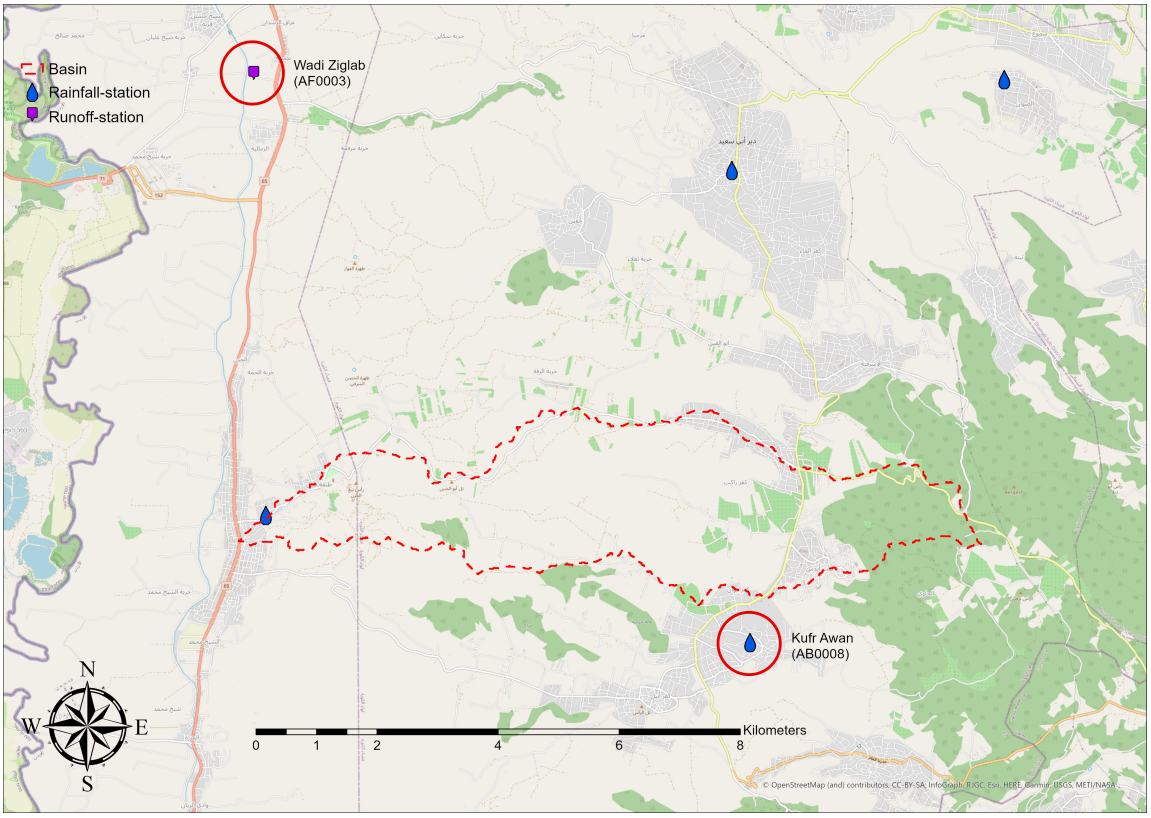

Figure 3.2: Nearby rainfall- and runoff stations.

factor that influences the curve number. This is classified in three Antecedent Moisture Conditions (AMC): I, II, III, indicating, respectively, dry to saturated antecedent conditions. Since it concerns a semi-arid region, AMC I was selected.

For land use, ESA-Worldcover (2020) was utilised. This landcover map has a spatial resolution of 10 m. A quick observation of the dataset shows that the six main land covers in the selected wadi are:

- Forest
- Shrubland
- Grassland (redefined as: 'Grass dominated rangeland')
- Cropland
- Built-up
- Bare / sparse vegetation (redefined as: Bare soil)

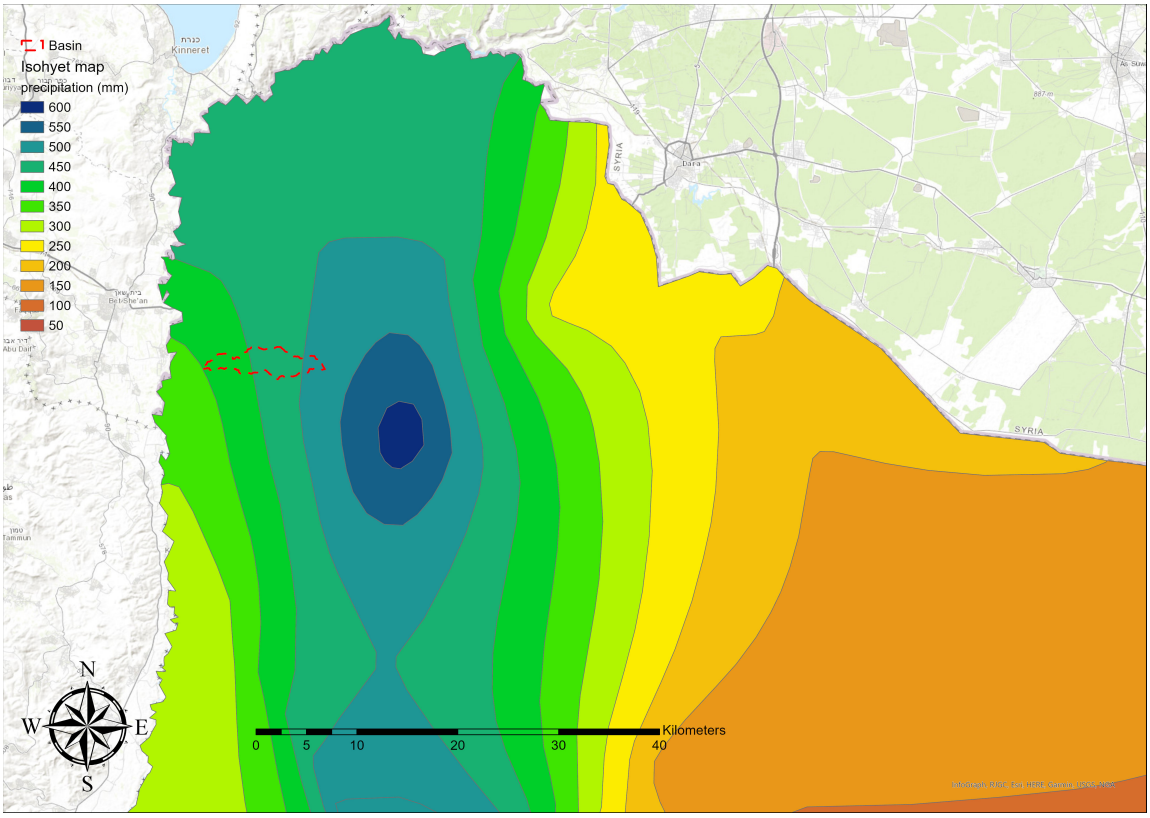

Figure 3.3: Isohyet map; precipitation (mm). Adopted from Jordan Meteorological Department (edited).

Definitions of the classes can be found in Appendix D. Additionally, a visual comparison of the cover map with Google Earth Pro (GE) open-source aerial imagery revealed that the wadi contains many olive orchards which were wrongly classified as forest. Therefore, they were manually digitized as polygons in ArcGIS Pro (GIS) (Esri-Inc., 2021) and merged with the ESA-Worldcover (2020) map, resulting in a total of seven land cover classes.

HSG's were taken from Ross et al. (2018). The map has a spatial resolution of 250 m. Using the Resample Tool (nearest neighbour) in GIS, the output cell size was decreased to match the land cover map. The wadi appears dominated by HSG-C and HSG-D. These groups represent, respectively, moderately high and high runoff potential. Descriptions can be found in the USDA classification scheme of HSG's.

The combination of land use and HSG's resulted in 14 Hydrologic Response Units (HRU)'s with varying CN's. These CN's were based on literature findings (Cronshey, 1986; Shammout et al., 2018; Akbari et al., 2021; Romero et al., 2007). Together with the rainfall data from the Wadi Ziglab station, the areas covered by the corresponding HRU's were multiplied with their assigned CN to obtain runoff quantities of the wadi, according to equations 3.1 and 3.2 (Jabri and Hessane, 2020).

FAO pond

To roughly estimate quantities of soil loss, the volume change of a water collection pond of the Food and Agriculture Organization of the United Nations (FAO) at Al-Mashari' was measured (UN, 2021). Due to soil loss, clogging has taken place over the past few years. Filling volume was estimated by comparing current height of the sediment in the pond, with the curbs and/or culvert as a reference point, to starting values found in drawings requested from the FAO.

3.3 Erosion hotspot mapping and field data collection

3.3.1 Step 1: Erodibility classification

An erosion hotspot map was created in order to identify prone and restorable areas in the wadi. This was done by determining potential erodibility of the soil and erosivity of runoff on certain HRU's. The calculated CN's were used for the latter. Erodibility was based on slope steepness, land cover and soil texture (Zhang et al., 2013; Alkharabsheh et al., 2013; Wang et al., 2013; Bonilla and Johnson, 2012). Slope steepness was retrieved from the ALOS-PALSAR (2009) elevation model, with a spatial resolution of 12,5 m. Land cover was taken from ESA-Worldcover (2020) (10 m) and soil texture from ISRIC (2017) (250 m). Before combining them, all factors were divided independently into three classes of erodibility:

1. Minor erodibility
2. Medium erodibility
3. Severe erodibility

First, the digital elevation model (DEM) showed some NoData values that needed to be resolved. This was done with the Raster Calculator tool. NoData values were filled with the average value of the neighbouring cells that do contain a value. Slope categories were divided in 0 - 10°, 10° - 20° and $\geq$ 20° (Farhan et al., 2013).

As silt is highly detachable, soils with high silt content are most prone to erosion, especially when this content exceeds 40% (Morgan, 2009; Richter and Negendank, 1977; Pérez-Rodríguez et al., 2007; Bonilla and Johnson, 2012). To obtain silt content, values of three ISRIC (2017) silt content maps at depths of 5, 15 and 30 cm were averaged in GIS with the Raster Calculator tool. The approximate depth were rills become gullies is 30 cm, hence the decision to average the first 30 cm of silt content. The increase in rill erodibility as a function of silt content is exponential. However, below 65% this increase is not yet major (Figure 3.4). As the averaged silt contents ranged from 30% - 47%, they were only appointed to erodibility class 1 and class 2 with a range of, respectively, 30% - 40% and $\geq$40%.

According to Wang et al. (2019) and İlay and Kavdir (2018), the land cover forest and shrubland have minimum soil erodibility. This is followed by olive orchards and grasslands, and maximum erodibility for croplands. For the erosion hotspot classification, built-up area was added to class 1. Shrubland, however, was moved to class 2. According to the ESA-Worldcover (2020) classification (Appendix D) shrubland in this map is defined as "any geographic area dominated by natural shrubs having a cover of 10% or more". Visual comparison of the designated shrublands with GE aerial images exposed that the shrublands in the selected wadi are poorly covered and the assumption was made that its erodibility is significantly higher than forests and built-up. Grass dominated

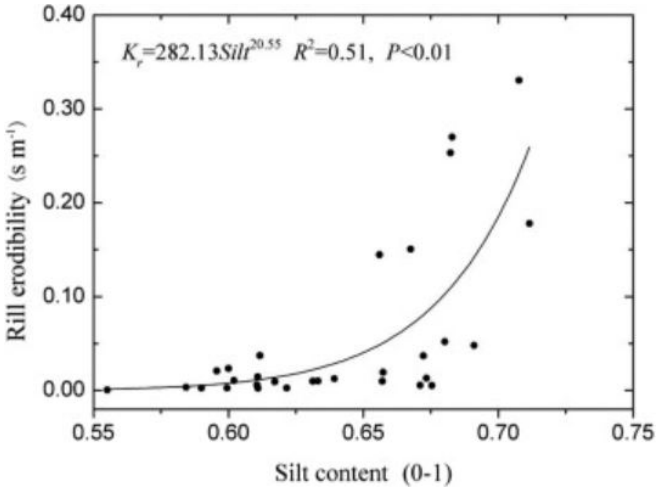

Figure 3.4: Rill erodibility (K_r) as a function of silt content. Adopted from Li et al. (2015)

rangelands, olive orchards and croplands were assigned to class 2 and bare soil to class 3. Likewise, it was assumed that erodibility differences between croplands and bare soils are larger than those between croplands and the other appointed class 2 land covers.

Finally, the classified factors were given a certain weight and were combined to form the erosion hotspot map. According to Zhang et al. (2013), Runoff erosivity and vegetation coverage are most significant in contributing to soil erosion, followed by slope and soil type. Since silt has little variation it was also assumed that its impact on erodibility is smallest and its weight was set to 0,2. Runoff erosivity was accounted for by the CN. Since silt variation is small, the major variability in erodibility in the CN approach lies in the land cover which is integrated in the CN calculation. Since land cover and runoff erosivity were considered most significant, they were given a weight of respectively 0,3 and 0,2, resulting in a largest summed weight for land cover. This was followed by slope, with a second largest weight of 0,3. A final factor that needed to be accounted for is the slope aspect (Figure 3.5). In the Northern Hemisphere, southward facing

Figure 3.5: Condition differences between north- and south facing slopes. Date: December, 2021.

slopes receive more solar radiation and are often hotter and drier, resulting in less vegetation and increased susceptibility to soil erosion (Burnett et al., 2008; Bochet et al., 2009; Farhan et al., 2014). Hence, northward facing slopes were given an additional weight of -0,1 while southward facing slopes remained unchanged. Fields visits to various hotspots and GE imagery were used to visually validate the hotspot classification.

3.3.2 Step 2: Restoration potential

The second step was to filter out non-restorable areas. These comprise occupied areas which have agricultural purposes (croplands, olive orchards) and areas where restoration is illogical or impossible (built-up, forests). The remaining coverage (shrubland, grass dominated rangeland, bare soil) was considered restorable. This was filtered in GIS using the ESA-Worldcover (2020) classification. The restoration measures will consist of the manual plantation of trees. At request of project leader Dr. Strohmeier the steepness of slopes was not integrated as a limiting factor for restoration activities. While, for example, the 'Vallerani Delfino-Plow' system would only be able to plow at slopes up to 14° (Strohmeier et al., 2021; Vallerani-System, 2022), manual plantation will allow more acreage to be restorable whilst targeting steep and thus prone slopes.

3.3.3 Step 3: Field data collection

Additional fieldwork was required for accurate modelling with RHEM. The parameter values to be collected were:

- Soil texture
- Cover characteristics
- Rill density
- Slope length and shape

Slope steepness for chosen locations was estimated by a slope map produced in GIS and roughly checked in the field with use of an inclinometer. The data collection sites were selected based on the produced erosion hotspot map. Three representative and restorable areas were chosen for erodibility class 3, two areas for class 2 and one area for class 1. Class 1 was expected to have little to no contribution to soil loss, but a quick field assessment was desired anyhow to validate this, to validate the hotspot map classification, and to obtain some cover characteristics for non-eroded areas. Selection was also based on accessibility by car and foot, which was often challenging due to unpaved/muddy roads, topography, unexpected fencing, etc.

Soil texture was predefined using ISRIC (2017) data and validated by an organoleptic assessment in the field. The predefined soil textures were obtained by looking at sand-, silt- and clay fraction at 5 cm depth (ISRIC, 2017). Then, soil texture was determined following the soil texture triangle (Figure 3.6) (Shirazi and Boersma, 1984) The organoleptic assessment followed the flow diagram (Appendix E) of texture feel analysis by Thien (1979). For these estimates, two disturbed soil samples at 5 cm depth were taken at each selected hotspot at approximately $\frac{1}{3}$th and $\frac{2}{3}$th of the slope.

Next, a plant- and ground cover assessment was performed at the selected sites. Input parameters for RHEM are:

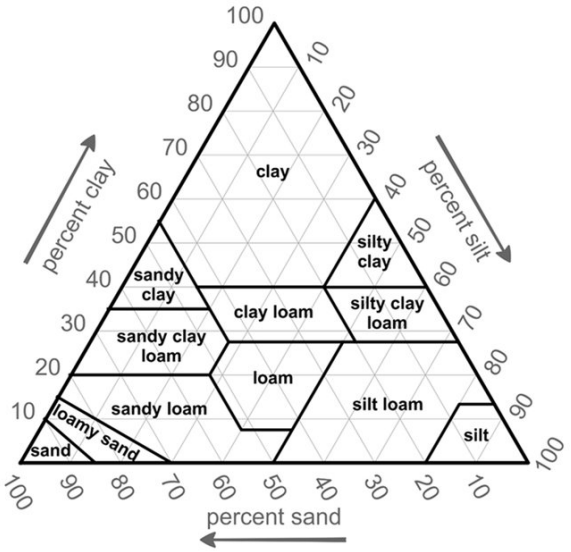

Figure 3.6: USDA Soil Texture Triangle

Plant cover

- bunchgrass
- forbs/annual grass
- shrubs
- sod grass

Ground cover

- Basal plant cover
- Rock cover
- Litter cover
- Biological crust cover

A rapid and accurate method for quantifying plant- and ground cover is the line-point intercept method Herrick (2005). A measuring tape of 50 meter was spanned to perform a point analysis at every 50 cm with use of a pointer. This procedure was performed twice: once aligned with the slope, once perpendicular to the slope. Plant cover was measured as the first hit from above. The first hit on material that is in contact with the ground itself was considered ground cover. Additionally, several photographs were taken per site in case of unexpected results. A detailed description of the line-point intercept procedure can be found in Herrick (2005). The sampling template is attached in Appendix F.

Next to this soil texture and cover assessment, rill density and slope shape were determined were possible. Choices for slope shape were: uniform, concave, convex and s-shaped (combination of convex to uniform to concave). Uniform slopes tend to produce most runoff and soil loss and concave slopes tend to produce the least. Spatial variability in soil loss between concave and convex slopes, however, remains rather unclear (Sensoy and Kara, 2014). If rills were visible, an estimate of their density and depth was made and noted using measuring tape as the severity of the features provide feedback on erosion occurrence at the classified risk zone. A more extensive rill density assessment was included in the stream network analysis (section 3.3.4), where slope length was

approached.

3.3.4 Step 4: Stream network assessment

A stream network assessment was put together to yield slope lengths that are most likely to occur with given slope steepness. This was done so that representative and generalized RHEM scenarios could be created whose output were out-scaled to wadi-level.

First of all, areas of interest were selected with the use of GE imagery and an aspect map created from the DEM for slope/flow direction. These areas comprise gully-rich areas. GE's measuring tools, 'Path' and 'Elevation profile', were used to estimate slope lengths and slope steepness. Slope lengths were measured from the top of the hillslope, following the flow path, down to the head of the gully. Thereafter, the locations were retrieved, checked and supplemented by more measurements in the field using a handheld GPS (Garmin Montana 650) with a general positional accuracy of within 5 to 10 meters under normal conditions (Garmin-Support, 2022). With the GPS, measurements were taken at, what appeared to be, the top of the slope and at the gully head. In case of agreement, more GE measurements could be added afterwards. The GPS points were converted to features, and features to KML in order to display the GPS points in, respectively, GIS and GE.

These field visits also included a rill density assessment. Where detectable, the densities and depths of rills leading up to a gully were measured. RHEM has set the rill density to 1 m by

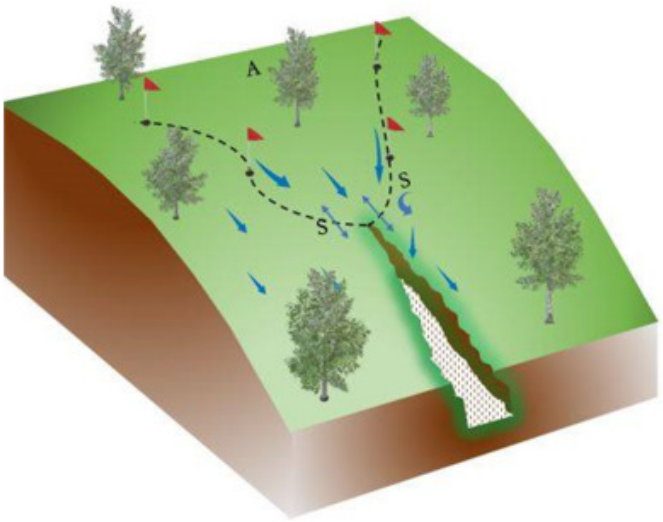

Figure 3.7: Schematic representation of upstream drainage area (A), delimited by red flags and dashed line. Arrows indicate runoff direction. Adopted from Yibeltal et al. (2019)

default during modelling. The rill density assessment was performed to either justify or improve the accurateness of this choice.

The average of the yielded slope lengths was used to approach the threshold upstream runoff drainage area (m^2) before a gully head starts (Figure 3.7). It was assumed that this area has a triangular shape. The resulting area was divided by the pixel size of the DEM to obtain the number of pixels required to form a stream. This threshold was applied to a flow accumulation map created

in from the DEM in GIS. (Figure 3.8) The ensuing stream network was compared with the aerial imagery of GE to see whether it matches the gullies in the measured areas sufficiently, in order to justify the measured slope lengths.

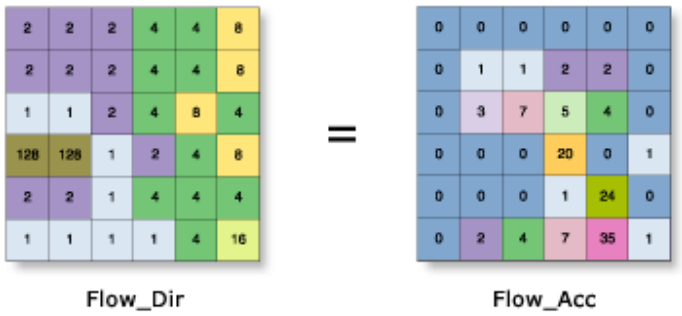

Figure 3.8: Flow Accumulation is a raster of accumulated flow to each cell, as determined by accumulating the weight for all cells that flow into each downslope cell. Adopted from `https://pro.arcgis.com/en/pro-app/latest/tool-reference/spatial-analyst/flow-accumulation.htm`

Then, a correlation- and regression analysis was performed on the collected slope steepness and -lengths. Normality was assessed by means of a frequency distribution, skewness and by comparing mean and median. As the data was roughly normally distributed and appeared linear, the Pearson correlation coefficient (equation 3.3) was consulted to examine the correlation and its significance (StatisticsSolutions, 2021; Statology, 2021).

$$r_{xy} = \frac{n\sum x_i y_i - \sum x_i \sum y_i}{\sqrt{n\sum x_i^2 - (\sum x_i)^2}\sqrt{n\sum y_i^2 - (\sum y_i)^2}} \tag{3.3}$$

r_xy = Pearson r correlation coefficient between x and y
n = number of observations
x_i = value of x (for ith observation)
y_i = value of y (for ith observation)

After significance of the correlation was indicated, the equation of the corresponding regression line was applied to the accumulative slope map values of the wadi to retrieve dominant slope length combinations.

3.4 Composing and running RHEM scenarios

3.4.1 Initial degraded and restored equilibrium phase

Runoff and soil loss of the current degraded wadi were approximated by composing and combining six RHEM scenarios, varying in slope steepness and -length, cover characteristics and soil texture. Slope steepness and -length were based on results of the stream network analysis (section 3.3.4). Cover characteristics were taken from the average line-point intercept results gathered for hotspot class 1, 2 and 3. From these slope- and cover characteristics, three scenarios were composed which were run for the two dominant soil textures described in section 3.3.1.

In an ideal future scenario, the erosion hotspots in the wadi would be restored, resulting in a balance between water erosion and the ecosystem's resilience. To simulate this, it was assumed that vegetation cover of hotspots class 2 and 3 resemble that of class 1. Restoration pits have been filled up by sediment so their sediment capture and storage capacity has diminished. In this combination of scenarios, the defined hotspot class 1 areas remained unaltered. Additionally, non-restorable acreage, as defined in section 3.3.2, was filtered from hotspot class 2 and 3.

After the scenarios were composed, the variables were entered in the online RHEM interface to prepare the input files (.par) per scenario. A choice of rainfall station is required to compose the input parameter file, but it is irrelevant which one this is. The nearest station (Jerusalem Central) was chosen. The rainfall data from the Kufr Awan station was used to bias correct CLIGEN. Preparation of the GDS file required not only rainfall data, but also daily minimum and maximum temperature data (°C). Therefore, temperature data was extracted from the National Oceanic and Atmospheric Administration (NOAA) for the IRBID meteorological station (ID: 40255099999) (NOAA, 2006). Data gaps were interpolated in Excel using the first available measurement before and after the gap. After the CLIGEN storm file (.out) was generated, RHEM was executed by means of a command line option file (kin.fil), in which the parameter input file, the storm file, and the output file name can be specified. This was repeated for all scenarios.

3.4.2 Impact assessment of WH structures

Immediately after implementation of water harvesting (WH) structures, the pits have a maximum water- and soil capturing capacity while vegetation is still in its degraded state (Figure 3.9). If the

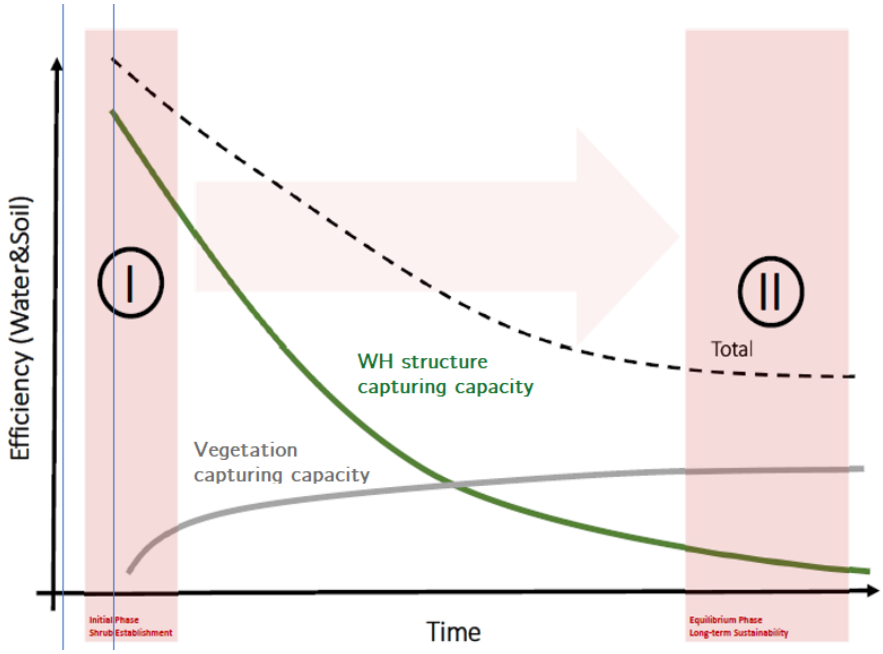

Figure 3.9: Water and soil capturing efficiency: The concept of direct and long term capturing efficiency of WH structures and corresponding vegetation.

structures were to capture too much runoff, this would have negative consequences for downstream areas as they become water deprived. Therefore, the output of the initial degraded scenarios was post-processed using a Python script to quantify the immediate impact of WH structures regarding runoff capturing capacity (RCC) and sediment capturing capacity (SCC). Using this quantitative assessment of the runoff water and sediment buffer capacity, land management is capable of designing the most optimal pit dimensions and determine the suited interspaces for the restoration project.

Runoff capturing capacity

The intended structures for the pilot field of the project, designed by ICARDA, have a top-view wet area of 0,25 m^2, a depth of 0,2 m and a volume of 50 liter (= 50 $\frac{mm}{m^2}$) (Figure 3.10). The plot size per

Figure 3.10: Pilot field for tree pit structures

structure is 3 x 3 = 9 m^2. It was assumed that approximately 10% of the area will be unsuitable for structures due to rock cover, resulting in 1000 potential structures per hectare (ha). Subsequently, there would be an average RCC of 5 $\frac{mm}{m^2}$ when the pits are empty. It was also assumed that the pits fill uniformly with runoff. Basic infiltration rate of the soil in the pit was presumed to be 10 $\frac{mm}{h}$. Taking into account that finer sediments accumulate in the pit, this rate was, conservatively, set to 7,5 $\frac{mm}{h}$ infiltration in the pits, thus taking over 26 hours for a full pit to empty. This means that per plot of 9 m^2 with one pit, an average of 4,5 $\frac{mm}{m^2}$ of water can infiltrate per day. This is assuming that water only infiltrates in the pits and excluding the 10% presumably unsuitable area (Salazar et al., 1994; Ghazal and Yasin, 2021). In case of consecutive days of runoff generation, there was accounted for residual standing water in the pits as it decreases their remaining capturing capacity. It was assumed that water might not always flow directly into the next pit below, but perhaps flow in between two pits into the next lower pit. This would increase the plot size to 3 x 6 = 18 m^2. Therefore, the script was also run for a halved RCC and infiltration rate. Subsequently, their outcome was averaged.

Sediment capturing capacity

Besides runoff, the pits also capture sediment as the standing water allows for suspended sediments to settle. To roughly estimate the SCC of the pilot pits, the RCC script was extended. A second order polynomial trapping efficiency (TE) function was computed per scenario. It was assumed that 99% of the soil loss could be captured during the minimum runoff event of a specific scenario. It was also assumed that only sand particles were captured during the 25 year return period runoff event of each scenario, after which the TE would flatten. The input for these equations was the excess runoff. The excess runoff was calculated in the RCC script, which was the runoff not captured by the pits. This was multiplied by the soil loss to obtain the average amount of sediment captured.

Chapter 4

Results

This chapter presents the results obtained to quantify surface runoff and soil loss in the selected wadi, as well as identifying its erosion hotspots and potential restorable areas. First, the results of the hydrological pre-assessment are presented, followed by the erodibility map. Next are the results of the additional field data collection required for RHEM input, and the RHEM modelling results. Finally, results for the direct impact assessment of WH structures is presented.

4.1 Pre-diagnostics of the selected wadi

Runoff: curve number

The CN approach was used to assess runoff erosivity in the wadi. Figure 4.1 presents the HSG map, land cover map and the resulting HRU map which were used for the CN runoff calculations. The corresponding CN's and their coverage were defined as in Table 4.1. Average annual precipitation

HRU	Area (m^2)	Land cover	HSG	CN	Erosivity class	Average annual runoff ($\frac{mm}{m^2}$)
1	432159	cropland	D	81	2	48,5
2	1030785	built-up	D	95	3	207,0
3	12403364	grass dominated rangeland	D	88	2	97,0
4	2079195	olive orchard	D	81	2	48,5
5	2984119	grass dominated rangeland	C	84	2	65,2
6	794207	shrubland	D	83	2	59,0
7	353953	bare soil	D	94	3	183,9
8	162158	bare soil	C	91	3	132,2
9	632702	forest	D	91	1	39,8
10	163986	built-up	C	79	3	183,9
11	172603	olive orchard	C	94	1	29,5
12	763786	shrubland	C	76	1	32,6
13	964982	forest	C	73	1	21,7
14	83429	cropland	C	78	1	36,0

Table 4.1: CN runoff calculations.

in the wadi, based on the 39 years daily rainfall data record of Kufr Awan station, was 448,9 mm.

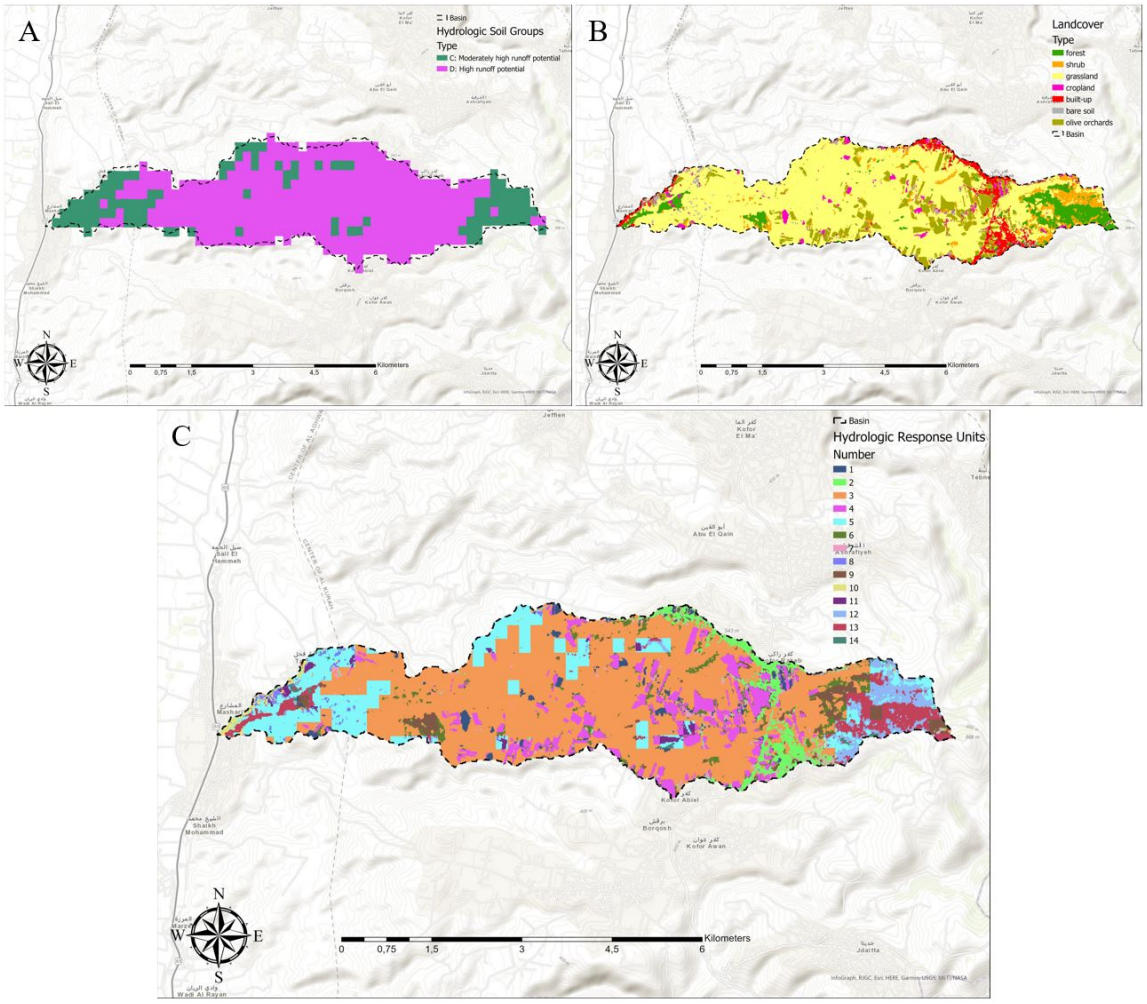

Figure 4.1: A: Hydrologic Soil Groups, B: Land cover including the digitized olive orchards, C: The resulting Hydrologic Response Units.

This resulted in an average annual runoff of 85,8 mm and a runoff ratio of 19,1% in the wadi. The average runoff ratio for the entire Northern side wadis basin, obtained from the MWI Water Budget report, was 6,1%. In case of rainy days, average daily rates measured at the Kufr Awan station ranged from 14 mm per event in December to no rainy days recorded at all in July to September of 1980-2018 (Figure 4.2). During this time span, there were 28 recordings of heavy precipitation days of > 50 mm. The most extreme rainy day was measured on February 2, 1985, when 123 mm was recorded.

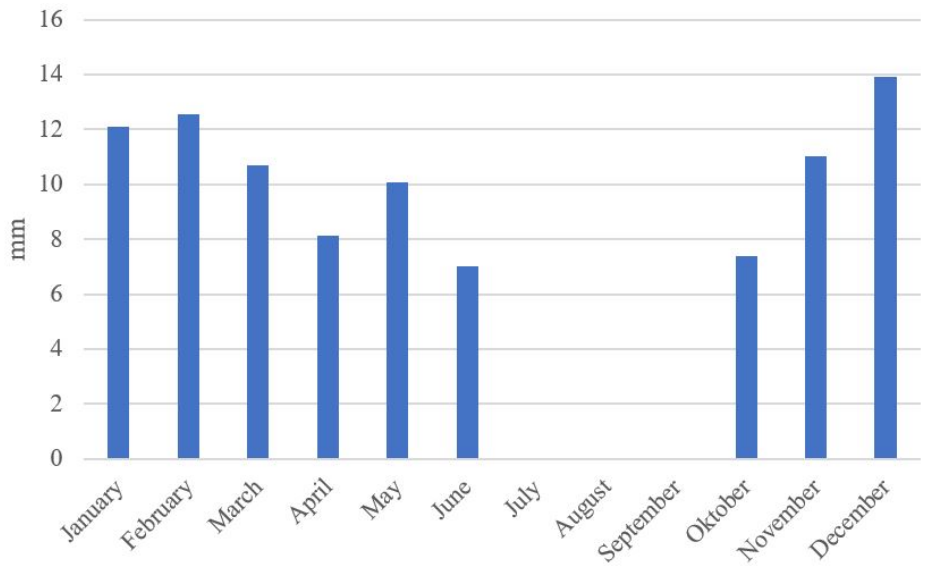

Figure 4.2: Average rain event (mm/day), Kufr Awan station (1980-2018).

Soil loss: FAO pond

Sketches containing specifications of the FAO pond were collected, among them the construction depths. The culvert could not be retrieved in the sketches and was therefore discarded as a reference point. Upon arrival, the FAO pond appeared to be, unexpected, full of water. This made it impossible to measure sediment level in the pond relative to the curbs as well. As a result, the pond could not be used for soil loss validation purposes.

4.2 Erodibility map

The erosion hotspot map was composed in accordance with the method described in section 3.3.1. A flowchart of the final hotspot mapping procedure was demonstrated in Figure 4.3, and the resulting erosion hotspot map in Figure 4.4B. An aerial overview was included for comparison (A). In Figure 4.4C, the non-restorable areas as was defined in section 3.3.2 are filtered out. It also includes the sites that were selected for additional field data collection and visual hotspot validation (section 3.3.3). According to this classification and based on the amount of pixels per class, 25% of the wadi is at low risk of erosion, 53% is prone to medium erosion and 22% is highly erodible. After removing the non-restorable areas, only 47% of the area of Class 1 remains and is considered restorable. For Class 2, this is 81% and of Class 3, 97% is restorable (Table 4.2).

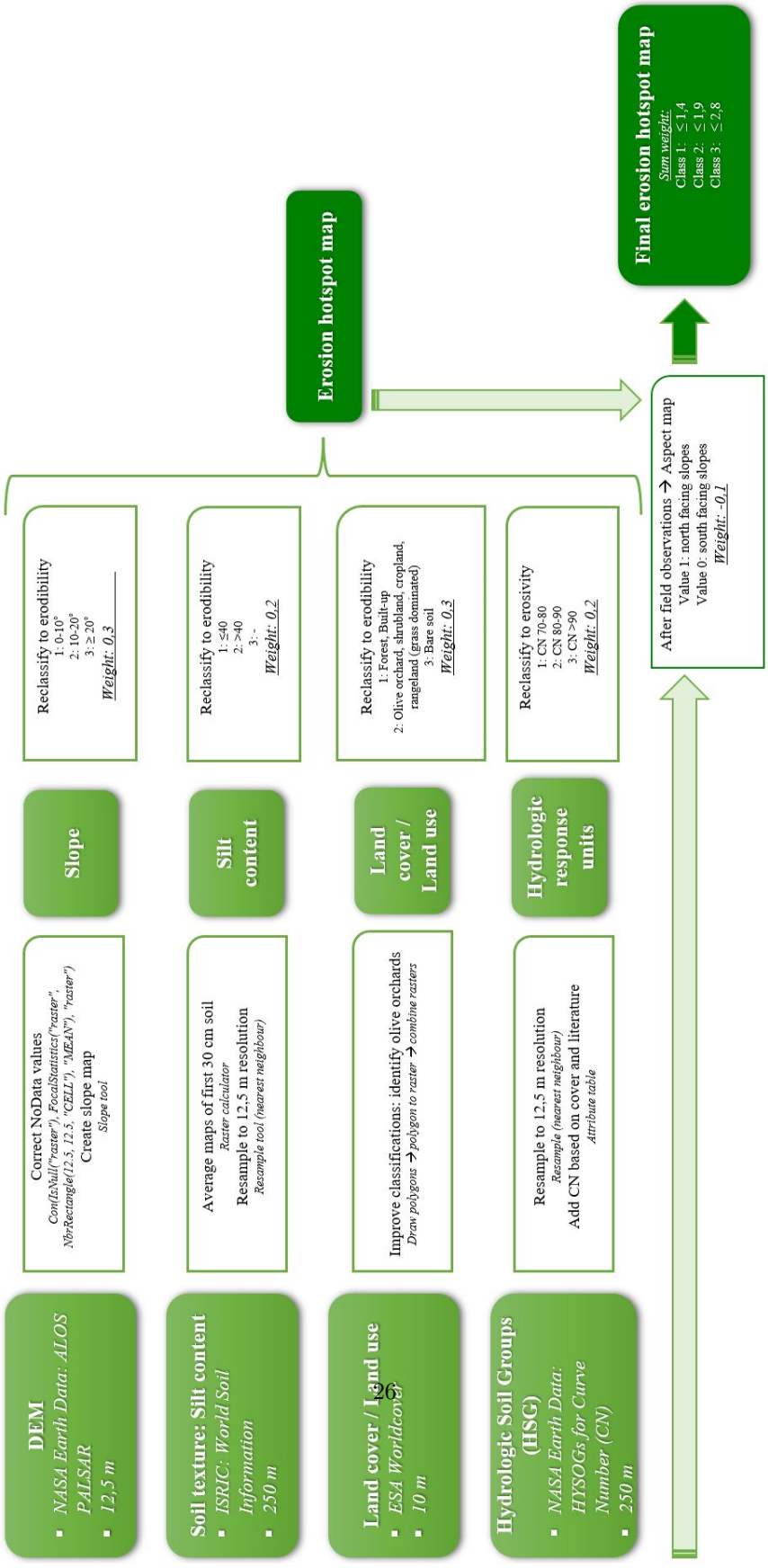

Figure 4.3: Flowchart of the erosion hotspot mapping procedure.

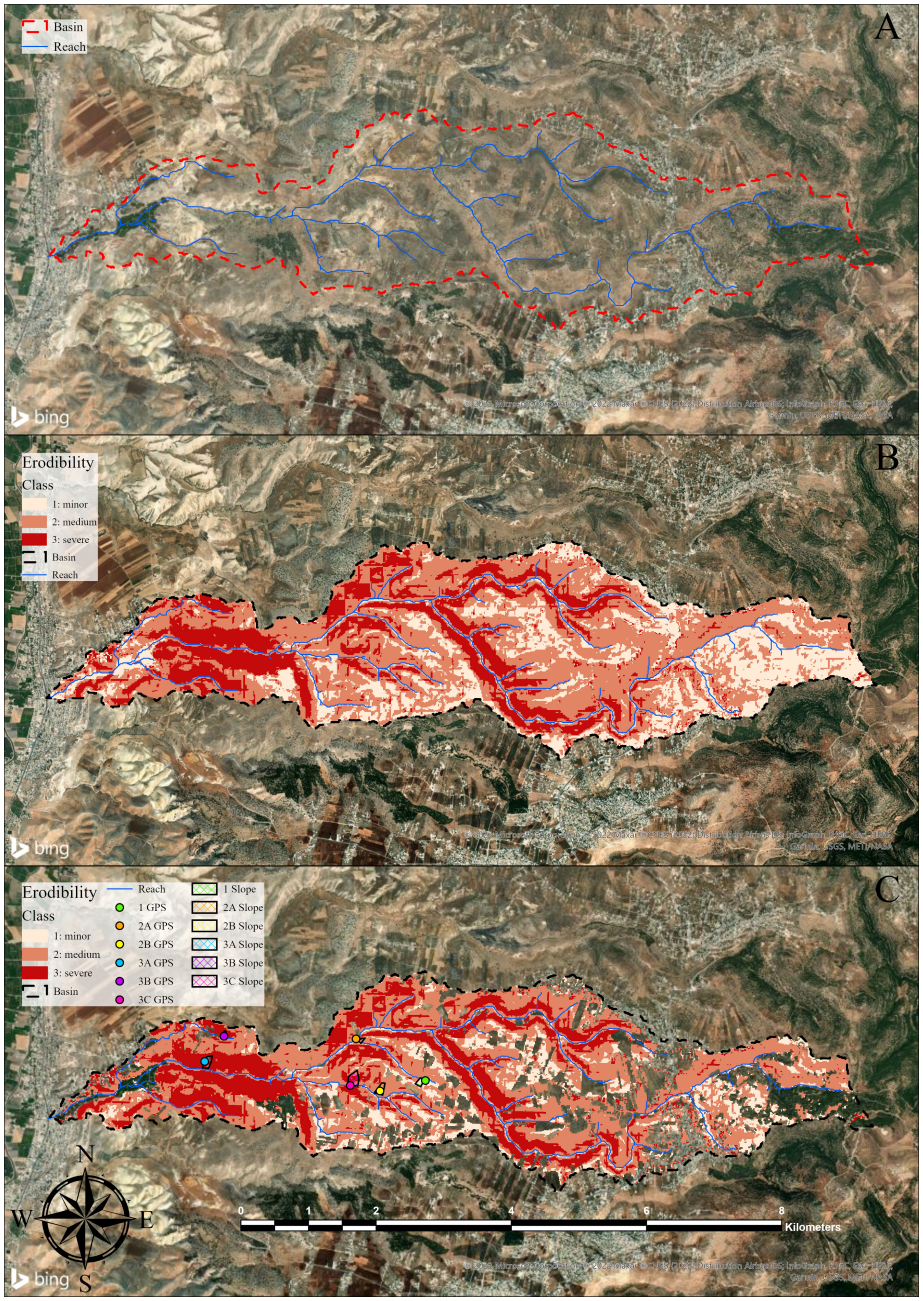

Figure 4.4: A: Classified erosion hotspots in the wadi, B: Aerial view of its true condition, C: Non-restorable areas filtered out; locations for hotspot verification and additional fieldwork.

Hotspot class	% of wadi acreage	ha	% restorable	% of wadi acreage restorable	ha
1	25	526	47	12	246
2	53	1115	81	43	902
3	22	463	97	21	450

Table 4.2: Erodibility class coverage

4.3 Field data collection

Soil texture

Clay-, silt- and sand fractions of ISRIC (2017) at the data collection sites resulted in soil textures that were predominantly clay loam and some silty clay loam (Table 4.3). This was reinforced by the organoleptic field assessment.

Hotspot ID	Coordinates	Clay %	Silt %	Sand %	Texture
1	35, 6549603°E; 32, 4463382°N	32	36	31	Clay loam
2A	35, 6456494°E; 32, 4519078°N	33	39	29	Clay loam
2B	35, 6486790°E; 32, 4453550°N	33	38	28	Clay loam
3A	35, 6213149°E; 32, 4489728°N	34	42	23	(Silty) clay loam
3B	35, 6239715°E; 32, 4528176°N	34	42	23	(Silty) clay loam
3C	35, 6444117°E; 32, 4466714°N	34	39	26	Clay loam

Table 4.3: Soil texture of the fieldwork sites.

Line-point intercept

Cover percentages per location and average percentages per class can be found in Table 4.4. Of the foliar cover, bunch grass, annual forbs and shrubs were found to be decreasing towards higher

	Foliar cover (%)				Ground cover (%)			
Hotspot ID	bunch grass	annual forbs	shrubs	sod grass	basal plant cover	rock cover	litter cover	biological crust cover
1	10,0	48,0	3,0	0,0	7,0	18,0	36,0	0,0
2A	2,8	7,7	6,8	0,0	1,5	18,8	15,9	10,3
2B	5,5	10,5	7,5	0,0	3,5	22,0	20,0	0,0
3A	1,0	2,0	0,0	0,0	0,0	42,5	10,5	0,0
3B	8,0	11,0	3,0	0,0	1,5	33,5	16,0	0,0
3C	1,0	0,5	7,5	0,0	0,5	37,0	12,5	0,0
Hotspot class	Average per class							
1	10,0	48,0	3,0	0,0	7,0	18,0	36,0	0,0
2	4,2	9,1	7,1	0,0	2,5	20,4	18,0	5,1
3	3,3	4,5	3,5	0,0	0,7	37,7	13,0	0,0

Table 4.4: Line-point intercept cover percentages

erodibility classes. Sod grass was not at all observed in the field. From ground cover, basal plant- and litter cover decreased towards higher erodibility classes while rock cover increased up to 42,5% (Figure 4.5). Biological crust cover was only observed at hotspot 2A.

Figure 4.5: High rock cover at site 3A

Slope shape

No dominant slope shape was discovered during the field visits. Observations showed mainly uniform-, convex- and combined (s-shaped) slopes, and few concave slopes (Figure 4.6).

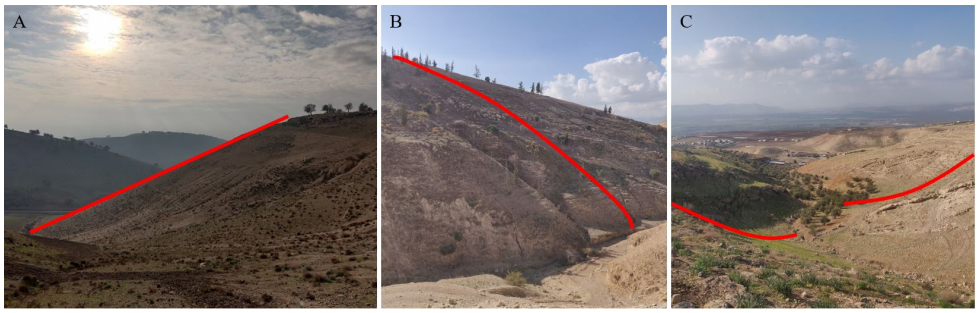

Figure 4.6: Examples of A: uniform-, B: convex- and C: concave slopes. Date: December, 2022.

For reasons of simplicity and triviality to this study, the uniform slope shape was chosen for all RHEM scenarios.

Stream network

The selected gullies that were visible in GE were mostly clustered in the western half of the wadi. A total of nine flow paths were successfully retrieved and validated in the field. The average slope length difference between the measurements in GE and the field-GPS measurement concerned 19%. This could mainly be attributed to the inability to physically reach the upper parts of some slopes, for example due to steepness or slippery soil. After this validation, the flowpath measurements were

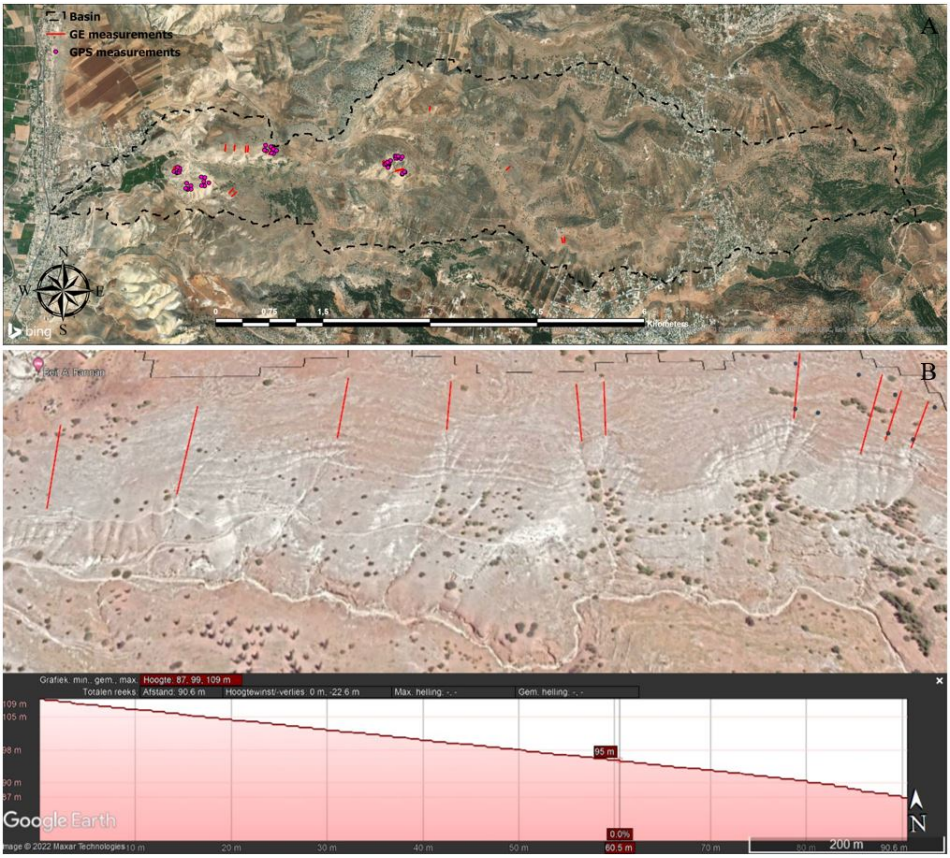

Figure 4.7: A: Overview of all flow path measurements, B: Use of GE (lines) and GPS (dots).

supplemented by an additional nineteen field measurements and ten measurements in GE, resulting in a total amount of 38, of which some were shown in Figure 4.7.

Rills prior to the gullies were measured only at ten occasions. Detectability was complicated mostly by (bed)rock and grazing paths (Figure 4.8). Average rill density was found to be 113,5 cm. During validation of the hotspots, rills were detected at site 3A, 3B, 3C and 2A. No rills were detected at site 2B and 1.

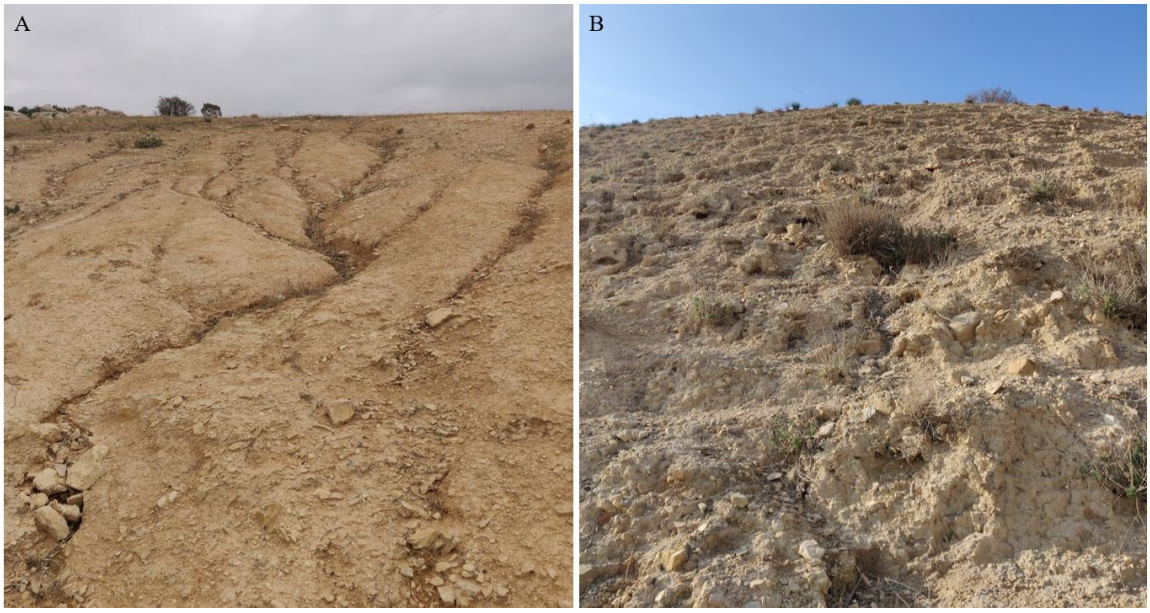

Figure 4.8: Good (A) and poor (B) detectability of rills. Date: January, 2022

The flow path measurements yielded an average slope length of 82,4 m which was considered equal to an average upstream drainage area of $\frac{82{,}4 \cdot 82{,}4}{2} = 0{,}34$ ha. The ensuing stream network with a threshold of 0,34 ha approximately matches the visible gullies in the measured sites (Figure 4.9). Other, less eroded areas, appeared overestimated. Most mismatches were related to factors not accounted for such as roads or land cover. Roads, and built-up in general, disturb natural flow paths, resulting in runoff concentration, interception and deviation (Nyssen et al., 2002). Since a land cover type such as forest is less susceptible to runoff erosion and would require a larger upstream drainage area to initiate gully erosion. Agricultural land undergoes plowing which can remove rills and ensuing gullies.

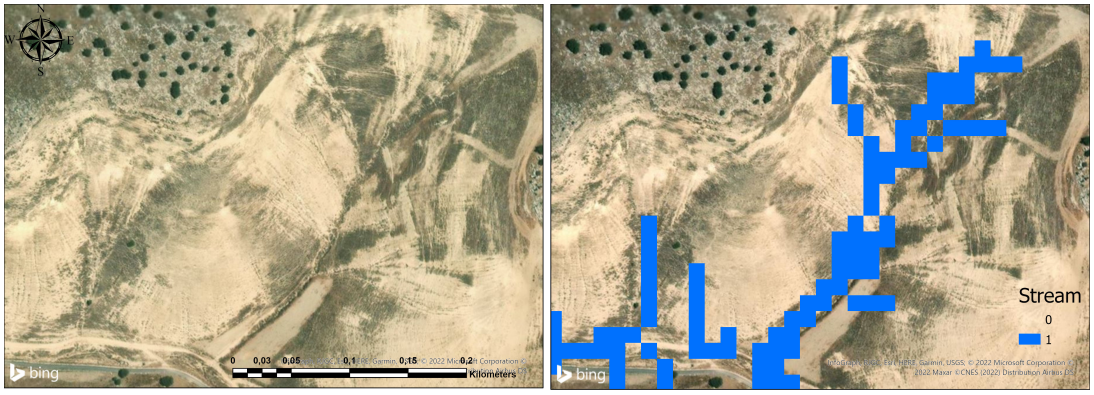

Figure 4.9: Stream network near hotspot 3C.

Slope steepness (y-axis) was plot as a function of slope length (x-axis) and rewritten to slope length as a function of slope steepness. This yielded the linear equation 4.1 with Root Mean Squared Error (RMSE) of 31,7 points.

$$y = 8,11688312 \cdot x - 46,42288961 \tag{4.1}$$

Slope length (y-axis) was also plot directly as a function of slope steepness (x-axis), yielding the linear equation 4.2 with a lower and therefore favoured RMSE of 19,5 points

$$y = 3,0495 \cdot x + 34,015 \tag{4.2}$$

Due to its lower RMSE, this equation was continued (Figure 4.10).

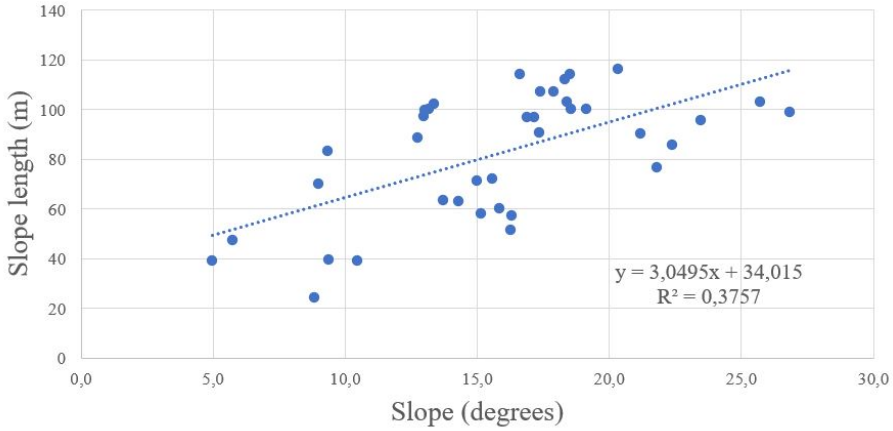

Figure 4.10: Slope length (y) as a function of slope steepness (x).

The Pearson correlation analysis yielded a coefficient of 0,613. Statistical significance of this correlation was indicated as the P-value of $4,3 \cdot 10^{-5}$ is less than the significance level (α) of 0,05 (Appendix G).

Regarding dominant slope length-steepness combinations in the wadi: Up to 25% of accumulative slope map values appeared to be below a slope of 10°, 50% were below 14° and the maximum slope value below 75% was 20°. Corresponding slope lengths found with the equation 4.2 were, respectively, 64,5 m, 76,7 m and 95,0 m. Correspondingly, these were further referred to as dominant slope-length combination (SLC) 1, 2 and 3.

4.4 RHEM modelling

The final scenarios that were composed for the RHEM modelling are described in Table 4.5. In the scenario codes, the first letter indicates whether in concerns either an initial degraded (D) or restored equilibrium (R) scenario. The following number (1, 2, 3) indicates the representative hotspot class regarding vegetation. Since the equilibrium scenarios consider all vegetation equal to hotspot class 1, without variation, these scenarios do not have a vegetation code. This is followed by either 10, 14 of 20 which stands for the chosen slope (°). Finally, 'A' stands for clay loam and

		SLOPE				FOLIAR COVER (%)				GROUND COVER (%)			
Scenario	Soil texture	Shape	Steepness (%)	Length (m)	Rill density (m)	Bunch grass	Annual forbs	Shrubs	Sod grass	Basal plant cover	Rock cover	Litter cover	Biological crust cover
D1-10A	clay loam	uniform	17,6	64,5	1	10,0	48,0	3,0	0,0	7,0	18,0	36,0	0,0
D1-10B	silty clay loam	uniform	17,6	64,5	1	10,0	48,0	3,0	0,0	7,0	18,0	36,0	0,0
D2-14A	clay loam	uniform	24,9	76,7	1	4,2	9,1	7,1	0,0	2,5	20,4	18,0	5,1
D2-14B	silty clay loam	uniform	24,9	76,7	1	4,2	9,1	7,1	0,0	2,5	20,4	18,0	5,1
D3-20A	clay loam	uniform	36,4	95,0	1	3,3	4,5	3,5	0,0	0,7	37,7	13,0	0,0
D3-20B	silty clay loam	uniform	36,4	95,0	1	3,3	4,5	3,5	0,0	0,7	37,7	13,0	0,0
R-14A	clay loam	uniform	24,9	76,7	1	10,0	48,0	3,0	0,0	7,0	18,0	36,0	0,0
R-14B	silty clay loam	uniform	24,9	76,7	1	10,0	48,0	3,0	0,0	7,0	18,0	36,0	0,0
R-20A	clay loam	uniform	36,4	95,0	1	10,0	48,0	3,0	0,0	7,0	18,0	36,0	0,0
R-20B	silty clay loam	uniform	36,4	95,0	1	10,0	48,0	3,0	0,0	7,0	18,0	36,0	0,0

Table 4.5: Input parameters of degraded (D)- and restored (R) RHEM scenarios

'B' for silty clay loam. After the scenario ID's, Table 4.5 presents the slope characteristics with the SLC's, followed by the cover characteristics according to Table 4.4 and section 3.4.1.

The sum of the first six scenarios comprise the current degraded status of the wadi according to equation 4.3:

$$\begin{aligned} &0,89 \cdot ((0,25 \cdot D1\text{-}10A) + (0,53 \cdot D2\text{-}14A) + (0,22 \cdot D3\text{-}20A)) + \\ &0,11 \cdot ((0,25 \cdot D1\text{-}10B) + (0,53 \cdot D2\text{-}14B) + (0,22 \cdot D3\text{-}20B)) \end{aligned} \tag{4.3}$$

In the equation there was accounted for the acreage that each hotspot covers, which was 25% for class 1, 53% for class 2 and 22% for class 3 (Table 4.2). Additionally, there was accounted for soil texture cover in the wadi, which was 89% clay loam and 11% silty clay loam ((ISRIC, 2017); Table 4.3).

The future restored conditions of the wadi were composed according to equation 4.4:

$$\begin{aligned} &0,89 \cdot ((0,25 \cdot D1\text{-}10A) + (0,53 \cdot (0,81 \cdot R\text{-}14A) + (0,19 \cdot D2\text{-}14A)) + (0,22 \cdot R\text{-}20A)) + \\ &0,11 \cdot ((0,25 \cdot D1\text{-}10B) + (0,53 \cdot (0,81 \cdot R\text{-}14B) + (0,19 \cdot D2\text{-}14B)) + (0,22 \cdot R\text{-}20B)) \end{aligned} \tag{4.4}$$

In this equation there was also accounted for the non-restorable percentage of hotspot class 2 and 3. Since current hotspot class 1 was considered not to be of interest for restoration, it was included in the equation as the original scenarios D1-10A and D1-10B.

The runoff and soil loss quantities for each scenario estimated by RHEM are shown in Table 4.6.

Scenario	Precipitation	Runoff	Soil loss	Sediment yield
	mm/y	*mm/y*	*ton/ha/y*	*ton/ha/y*
D1-10A	433	31,513	0,442	0,439
D1-10B	433	17,236	0,274	0,272
D2-14A	433	52,370	2,299	2,287
D2-14B	433	24,857	1,345	1,337
D3-20A	433	60,830	4,985	4,961
D3-20B	433	28,266	2,885	2,870
R-14A	433	31,364	0,689	0,684
R-14B	433	17,132	0,423	0,419
R-20A	433	31,054	1,289	1,278
R-20B	433	16,920	0,796	0,788

Table 4.6: RHEM output for the scenario runs.

Runoff increased towards higher erodibility classes and was higher for clay loam scenarios compared to silty clay loam scenarios. Soil loss also increased towards higher erodibility classes and

was lower for silty clay loam than for clay loam scenarios. Estimated average runoff, soil loss and sediment yield for the current degraded wadi, according to equation 4.3, were respectively: 46,23 mm/y, 2,31 ton/ha/y and 2,30 ton/ha/y. The corresponding runoff ratio was 10,67 %.

For the restored equilibrium wadi, following equation 4.4, these values were: 36,14 mm/y, 1,08 ton/ha/y and 1,07 ton/ha/y with a runoff ratio of 8,34 %. This is an average reduction for the entire wadi of 21,8% in runoff, 53,4% in soil loss and 53,5% in sediment yield. Looking at the restorable scenarios separately (D2-14A, D2-14B, D3-20A, D3-20B), the restored equilibrium scenarios (R-14A, R-14B, R-20A, R-20B) show a decrease of, respectively, 40,1, 31,1, 48,9 and 40,1% in runoff and 70,0, 68,6, 74,1 and 72,4% in soil loss.

4.5 Direct impact of WH structures

In accordance with the hotspot coverage (Table 4.2; 4.3), a sand particle percentage of 28% was used for the computation of the TE equations. The minimum- and the 25 year return period runoff events of the restorable scenarios yielded the following TE equations (Table 4.7), where the TE flattens and decreases a little more towards 26% for the 100 year return period:

Scenario	TE equation	RCC	SCC
D2-14A	y = 0,0002x2 - 0,0213x + 0,9899	34,24%	75,44%
D2-14B	y = 0,0002x2 - 0,0264x + 0,9893	36,11%	69,57%
D3-20A	y = 0,0001x2 - 0,0203x + 0,9899	33,65%	70,29%
D3-20B	y = 0,0002x2 - 0,0255x + 0,9893	35,80%	70,42%

Table 4.7: TE equations per scenario, where 'y' is the TE and 'x' the runoff, and corresponding reduce in runoff (RCC) and soil loss (SCC)

An example of what such TE function is shown in figure 4.11

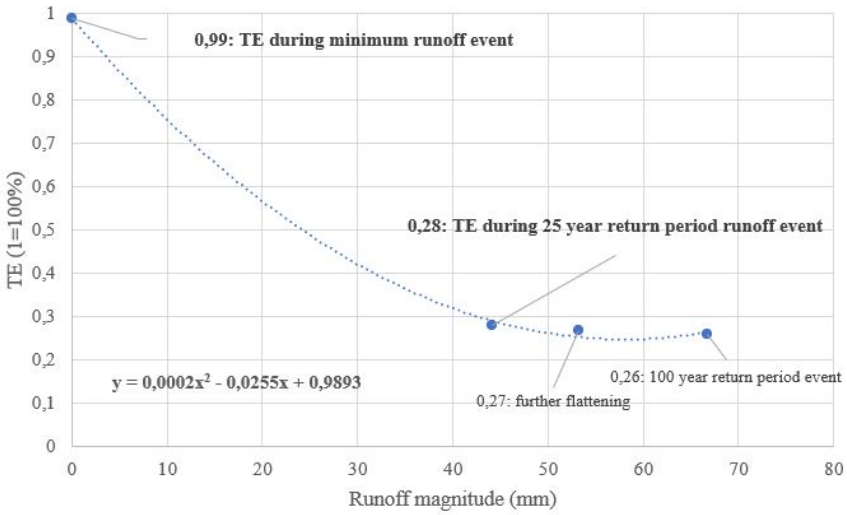

Figure 4.11: Second-order polynomial TE equation for scenario D3-20B

Table 4.7 also shows, for the restorable scenarios, the percentage of runoff and soil loss that was captured by the pits, which is the direct result of the implementation of WH structures. The reduce in runoff ranges between 33,65 - 36,11% and the reduce in soil loss ranges between 69,57 - 75,44%. The corresponding script was attached as Appendix B.3.

Chapter 5

Discussion

The research objectives which were proposed in the first chapter of this thesis are:

1. Hydrological pre-assessment of a selected side wadi for model validation.
2. Mapping of erosion hotspots and restorable areas for targeted future erosion control.
3. Quantification of runoff and soil loyss values in the wadi using RHEM for various scenarios;
    a. The current degraded phase
    b. The restored equilibrium phase
    c. The WH phase: a direct impact assessment of WH structures on runoff and soil loss in the degraded wadi.

This chapter discusses the corresponding obtained results (Chapter 4) in terms of importance, interpretation, uncertainty and recommendations. First, the produced erodibility map and is discussed (objective 2). Next is a section discussing the parameter input collection of RHEM, which was required for the runoff and soil loss quantification (objective 3a & b). Thereafter, modelled RHEM output (objective 3a & b) is discussed as well as the hydrological pre-assessment (objective 1). The final section is dedicated to WH impact assessment (objective 3c).

Erodibility map

The produced erodibility map was used as a basis for RHEM scenario definition and serves as a visualization of the severity of the degraded state of the wadi and its hotspots, stressing the need for erosion control. At the same time it emphasizes its potential regarding restoration of degraded ecosystems, which allows for targeted land management. Final classifications of the erodibility map that was produced for the selected wadi were based on slope steepness and -aspect, soil texture, land use and erosivity, retrieved from literature and pre-existing datasets (Figure 4.3). The resulting map implied that the majority of the area is prone to medium or even severe soil loss. From these prone areas, most was regarded restorable (Figure 4.4; Table 4.2). Visitations of some of these hotspots, as specified in Figure 4.4, showed that the sites appeared to follow the pre-classified sequence of erodibility, associated with steep slopes and extensive grazing paths. This was supported by declining foliar- and ground cover for the higher hotspot classes and the presence

of rills (section 4.3), indicating a higher erosion susceptibility. These local characteristics regarding erosion hotspots were in line with findings of Tamene et al. (2017) and Asmamaw and Mohammed (2019). It remains, however, difficult to make accuracy statements, since water erosion is a complex interplay of many factors of which only the independent effects were captured and summed in the hotspot map (Mosbahi et al., 2013).

RHEM parameter input collection

The input parameters of RHEM that were collected through fieldwork consisted of soil texture class, cover characteristics, slope characteristics and rill density. According to the ISRIC (2017) dataset, the soil texture class was clay loam and silty clay loam, which was confirmed by the organoleptic field test. A notable weakness of the ISRIC data is that its soil depth is always over 1 m. This was required for a good CN approach, yet unrealistic (too deep) for parts of the wadi. As predicted, silt content was lowest in the hotspot class 1 and increased towards class 2 and 3, indicating a higher erodibility (Table 4.3). However, these differences were small, with a maximum difference of 6%, and therefore considered not to be of great impact on erosion susceptibility. On the other hand, the differences between the sites might have been bigger in reality. The ISRIC dataset is of low spatial resolution and the organoleptic test is subjective and only suitable to roughly distinguish between texture classes, not to distinguish on a percentage level. It is recommended that disturbed samples be collected at a lower and upper part of the slope to retrieve average soil texture by means of the hydrometer method. This method calculates physical properties of soil particles based on their settling rate in an aqueous solution (Huluka and Miller, 2014).

Cover characteristics were determined with the line-point intercept method, and yielded a trend as expected: a decrease in foliar- and ground cover towards higher erodibility classes, leaving the soil vulnerable to raindrop impact and soil instability. An exception to this trend was rock cover, which was found to be increasing, with a maximum cover of 42,5% at site 3A. This appears contradictory as rock fragments protect the soil below it from rain splash erosion. On the other hand, a large rock cover as observed in the class 3 hotspot zones might trigger higher runoff rates and thus soil erosion (Yair, 2001). The study of Jomaa et al. (2012) also shows contradicting responses of rain splash erosion in the presence rock fragments under laboratory conditions versus field data. To make statements on the exact impact of the rock cover would require particular experiments or model runs focused on changing rock cover solely. Noteworthy is that all line-point intercepts were performed in late December, at the beginning of the rainy season and thus shortly after the dry period. Therefore it is recommended that similar measurements be taken later in the rainy season. Then, vegetation has started to regrow while the rain is still erosive. This would provide a better average impact of the vegetation cover on water erosion. A more accurate approach for future research would be to use drone imagery for classification of vegetation cover.

The stream network assessment yielded an average rill density of 113 cm and a function for the SLC's (Figure 4.10). The rill density of 113 cm approaches the default rill density of RHEM of 100 cm. Yet, as detectability was often poor and not convincing, the decision was made to retain the model default of 1 m to avoid too much subjectivity. Regarding the slope shape, no dominant slope shape was discovered during the field visits. Recommendation for future study would be to use higher resolution DEM's so that a GIS analysis can be performed using the slope Curvature Tool, which will yield slope shapes. The slope length measurements yielded an average slope length of 82,4 m and the average upstream drainage area was estimated to be 0,34 ha. The ensuing stream network was a lesser match to less eroded areas. This was considered acceptable as the eroded areas

are of interest to most runoff and erosion quantification. The yielded linear equation, presented in Figure 4.10, revealed a positive relation between slope steepness and length. This was somehow surprising as it was assumed that steeper slopes promote gully initiation (Desmet et al., 1999). The study of Vandaele et al. (1996) also indicates that the upslope drainage area decreases for steeper slopes. However, the positive linear relation between slope length and steepness does not explicitly indicate a larger upstream area. It might also be the case that the upstream sub-catchment shape becomes more narrow and therefore still smaller, which could be supported by increased density of gullies in the steep eroded areas such as in Figure 4.9.

RHEM output versus hydrological pre-assessment

The final composed model runs and their output were given in Table 4.5 and 4.6. An increased runoff and soil loss was observed for the higher erodibility classes. Additionally, runoff and soil loss were both lower for silty clay loam compared to clay loam scenarios. For runoff this makes sense, because silt has a higher infiltration capacity than clay. A lower soil loss for silty clay loam, however, seems contradicting, as silt is highly detachable and most prone to erosion (Morgan, 2009; Richter and Negendank, 1977; Pérez-Rodríguez et al., 2007; Bonilla and Johnson, 2012). And so it turns out that by looking at the ratio between the found soil loss quantities and the runoff quantities, the soil loss does indeed increase, yet relatively. The relative increase in soil loss between D1-10A and D1-10B is 13,5%, 23,3% between D2-14A and D2-14B and 24,5% between D3-20A and D3-20B (Table 4.6). This indicates that erosion susceptibility due to silt content increases as soils become steeper and/or more exposed.

The restored equilibrium scenarios showed an average reduction of 21,8% in runoff and 53,4% in soil loss for the entire wadi, emphasizing the potential impact a balanced ecosystem could have on runoff and soil loss quantities in these drylands. Though, in these scenarios the assumption was made that all restorable areas can be vegetated like scenario D1-10A. This is most likely overestimated as e.g. steep slopes or bedrock might complicate this for some areas. A more accurate estimate would require diverse vegetation scenarios, obtained by more extensive line-point intercepts throughout the wadi, or with the use of drone imagery classification.

The runoff ratio obtained by RHEM modelling was 10,67% for the current degraded wadi and 8,34% for the restored equilibrium wadi. The ratio for the degraded wadi was found to be higher than the ratio from the MWI Water Budget report, which was 6,1% for the entire Northern side wadis basin. This was considered to be in agreement with the found ratio, as the MWI ratio was calculated for the entire Northern side wadis, which also comprises lower rainfall zones while the Kufr Awan station of the selected wadi lies in a high rainfall zone (Figure 2.1A and 3.3). Compared to the CN calculated in the hydrological pre-assessment, with a runoff ratio of 19,1%, the ratio of 10,67% is low. This might be explained by multiple factors that could have caused overestimation. The first one is that the average rainfall produced by CLIGEN, 433 mm, was a little lower than the average rainfall from the Kufr Awan station, which was 449 mm. Secondly, the CN calculations did not include sub-hourly rainfall intensity, solely daily rainfall values. The summed precipitation volume at the end of a day might in cases have been enough to exceed the runoff threshold, while in reality there might have been low intensity rainfall spread over the day, not exceeding the runoff threshold. Finally, the CN calculation included built-up areas (Table 4.1), which produced among the highest runoff. Considering the above, the ratio of 10,67% for the current degraded wadi appears plausible.

Based on the study of Haddad et al. (2017) and on expert opinion of Dr. Strohmeier, current

soil loss in the wadi was expected to range between 2 and 20 tons per hectare. Thus, the modelled average soil loss of 2,31 ton/ha/y for the entire wadi and the maximum soil loss of 4,99 ton/ha/y for scenario D3-20A were considered rather low. This could be attributed to the high rock cover in the wadi, which was at an average of 37,7% for the class 3 areas such as scenario D3-20A (Table 4.4; Figure 4.5). To test this, rock cover of scenario D3-20A was lowered from 37,7% to 20%. This drastically increased soil loss from 4,99 to 11,6 ton/ha/y, which would be more in agreement with range found by Haddad et al. (2017) and Dr. Strohmeier. However, the decrease in soil loss found in the restored equilibrium scenario as compared to the degraded scenario (53,4%) is in line with findings of Haddad et al. (2022) on WH in the Jordan Badia. Here it was estimated that, if the Badia were to be restored, soil loss could reduce by 60,6%. Yet, it was still recommended to estimate the volume change in the FAO pond during a dry spell. This is, in combination with its contributing area, to approach its soil loss quantity as a validation. Also, additional fieldwork could determine whether the high rock content at the measures sites was representative or exceptional.

SCC and RCC of WH structures

The decrease in runoff and soil loss as a direct impact of WH structures was simulated by means of a python script, based on pit dimensions, infiltration rate and TE. The result is a (rough) tool for determining optimal pit dimensions and spacing. As described in Table 4.7 this yielded, for the restorable scenarios, an average decrease of 35% in runoff and 71% in soil loss, compared to the degraded scenarios. This decrease in soil loss in the WH scenario is nearly equal to the average decrease in soil loss of the restored equilibrium scenarios compared to the degraded scenarios, as described in section 4.4. The yielded average decrease in runoff compared to the degraded scenarios is 5% lower than the average 40% decrease of the restored equilibrium scenarios compared to the degraded scenarios. However, it was expected that the restored equilibrium scenarios would have a little higher sediment TE due to increased vegetation.
Most likely the TE of the pits was overestimated. Determining the exact TE of the pits would require further research on settling of the sediments under various conditions. A factor at play could for example be slope steepness, which was not accounted for in the script. Additionally, the computed TE equations were multiplied with the soil loss values calculated by RHEM for the entire slope. But since the runoff generation will be disrupted by the pits, these soil loss values might actually be overestimated, which simultaneously causes an overestimation of sediment trapping taking place.
It was also expected that the RCC during the WH phase would be highest as the pits have not been filled yet, but this was not the case. Either the pits should have larger dimensions, or the vegetation cover in the restored equilibrium scenarios was indeed overestimated, or both. Comparing runoff capturing efficiency of the structures to other studies is ambiguous, as there are multiple types of micro-catchment WH approaches, and even pits do not have fixed dimensions per study. However, the study from Oweis and Taimeh (1996) on small basin WH in Jordan found that mean efficiency was 51%, which approaches the efficiency found in this study. As RHEM considers evapotranspiration, it could be argued that the increased vegetation in the restored equilibrium phase empties the soil moisture storage quicker. This results in better uptake of following precipitation. Another explanation for these results could lie in the assumptions made in the python script, for reasons of simplicity. For instance, it was assumed that infiltration only occurs in the pits, while infiltration at the remaining plot size surface was not accounted for. If this were the case, the reduce in runoff would increase for the WH scenarios and perhaps still become lower than restored equilibrium sce-

narios. Thus, the script would require an improved runoff process description and corresponding input collection to properly simulate the direct impact of WH structures.

Chapter 6

Conclusion

The aim of this thesis was to study and quantify runoff and soil loss by water erosion in a Jordan side wadi during its current degraded state and after modelled implementation of rehabilitation measures. This ex-ante assessment was desired for the SIDA-FAO project to identify erosion hotspots and restorable sites, and to appraise direct and long term effects if restoration measures were to be implemented on large scale.

The northern Jordan side wadi that was selected is characterized dominantly by a degraded landscape. The produced erodibility map to identify erosion hotspots implied that the majority of the wadi is prone to medium (53% surface area) or even severe (22% surface area) soil loss. Simultaneously, the map emphasized that, respectively, 81% and 97% of surface area of these susceptible sites has potential for implementation of WH structures.

The hydrological pre-assessment, using the NRCS Runoff curve number approach and runoff/rainfall ratios, showed that average runoff ratio in the wadi was likely to lie in between 6,1% and 19,1%. The runoff and soil loss quantities of the wadi were modelled with the Rangeland Hydrology and Erosion Model (RHEM). Output of this model for the current degraded scenario was in agreement with the hydrological pre-assessment, as the sum of the degraded scenarios presented a runoff ratio of 10,7%. The soil loss sum for the degraded RHEM scenarios was 2,31 ton/ha/y, with maximum hotspots of 4,99 ton/ha/y. Based on field observations and expert opinion this was considered lower than expected. The assumption that was considered most likely is that this could be attributed to the high rock content in the high erosion class areas where input parameters for RHEM were collected.

The restored equilibrium RHEM scenarios which were explored gave an insight on achievable reduction in runoff and soil loss as a result of restoration measures. The scenarios yielded a runoff ratio of 8,34% and a soil loss of 1,08 ton/ha/y. This is a reduction of 21,8% in runoff and 53,4% in soil loss for the entire wadi, and an average reduction of, respectively, 40% and 71% for the restorable scenarios separately. It is likely that these percentages are the upper boundary of what is achievable due to impediments such as bedrock and slope. Still, the results substantiate a first quantification of the future ambitions of the project, emphasizing the impact of a better balance between water erosion and the ecosystem's resilience. It is also noteworthy that runoff and soil loss do not appear to decrease proportionally. The results indicate that, when vegetation cover of the wadi is in better equilibrium, soil loss might reduce over twice as much as runoff. This is a positive incentive to the project: the reduce of soil loss upstream, increasing soil productivity,

versus reducing runoff, depleting downstream areas of water, has a ratio of 2:1.

The direct impact of implementation of the suggested WH structures was assessed by means of a Python script and provides a rough tool for determining the optimal pit dimensions and spacing for the SIDA-FAO pilot fields. yielded the same decrease in soil loss as the restored equilibrium scenarios (71%) and a lesser decrease in runoff capturing capacity (35%). The TE was most likely overestimated, either by the computed TE equation and/or by using the original soil loss values for the entire slope, while in reality runoff generation and thus erosion would be disrupted by the pits. The runoff capturing capacity was likely underestimated in the WH phase due to an underestimated infiltration rate at the plots. Another explanation on why the RCC is higher for the restored equilibrium scenario could lie in the fact that RHEM considers evapotranspiration. As this scenario was characterized by high vegetation density, this would result in quick soil moisture storage emptying and higher uptake of following precipitation.

All together, the erodibility map stresses the current degraded state of the wadi, and its potential for restoration. The modelling output results emphasize that, if the wadi were to be restored, soil loss and runoff amounts would eventually decrease with respectively more soil being preserved for upstream areas than water is held back from downstream areas. This should incite local stakeholders' preparedness for uptake and out-scaling of restoration measures.

Bibliography

A. Akbari, F. Daryabor, A. Abu Samah, and Z. Shirmohammadi Aliakbarkhani. Improving runoff estimation by raster-based natural resources conservation service-curve number adjustment for a new initial abstraction ratio in semi-arid climates. *River Research and Applications*, 37(9): 1333–1342, 2021.

N. Al-Ansari, N. Alibrahiem, M. Alsaman, and S. Knutsson. Water supply network losses in jordan. *Journal of Water Resource and Protection*, 6(2):83–96, 2014.

O. Z. Al-Hamdan, F. B. Pierson, M. A. ing, C. J. Williams, J. J. Stone, P. R. Kormos, J. Boll, and M. A. Weltz. Concentrated flow erodibility for physically based erosion models: Temporal variability in disturbed and undisturbed rangelands. *Water Resources Research*, 48(7), 2012.

O. Z. Al-Hamdan, F. B. Pierson, M. A. Nearing, C. J. Williams, M. Hernandez, J. Boll, S. K. Nouwakpo, M. A. Weltz, and K. Spaeth. Developing a parameterization approach for soil erodibility for the rangeland hydrology and erosion model (rhem). *Transactions of the ASABE*, 60(1): 85–94, 2017.

A. S. Al-Omari, E. K. Al-Karablieh, Z. M. Al-Houri, A. Z. Salman, and R. A. Al-Weshah. Irrigation water management in the jordan valley under water scarcity. *Fresenius Environ Bull*, 24:1176–1188, 2015.

C. Alewell, P. Borrelli, K. Meusburger, and P. Panagos. Using the usle: Chances, challenges and limitations of soil erosion modelling. *International soil and water conservation research*, 7(3): 203–225, 2019.

M. M. Alkharabsheh, T. Alexandridis, G. Bilas, N. Misopolinos, and N. Silleos. Impact of land cover change on soil erosion hazard in northern jordan using remote sensing and gis. *Procedia Environmental Sciences*, 19:912–921, 2013.

L. AlMahasneh, D. Abuhamoor, K. Al Sane, and N. J. Haddad. Assessment and mapping of flash flood hazard severity in jordan. *International Journal of River Basin Management*, pages 1–15, 2021.

ALOS-PALSAR. Alos palsar digital elevation model (nasa), 2009. URL `https://search.asf.alaska.edu/#/?dataset=ALOS`.

L. B. Asmamaw and A. A. Mohammed. Identification of soil erosion hotspot areas for sustainable land management in the gerado catchment, north-eastern ethiopia. *Remote Sensing Applications: Society and Environment*, 13:306–317, 2019.

K. Auerswald, M. Kainz, and P. Fiener. Soil erosion potential of organic versus conventional farming evaluated by usle modelling of cropping statistics for agricultural districts in bavaria. *Soil use and Management*, 19(4):305–311, 2003.

C. Barrow. World atlas of desertification (united nations environment programme), edited by n. middleton and dsg thomas. edward arnold, london, 1992. isbn 0 340 55512 2,£ 89.50 (hardback), ix+ 69 pp. *Land Degradation & Development*, 3(4):249–249, 1992.

E. Bochet, P. García-Fayos, and J. Poesen. Topographic thresholds for plant colonization on semi-arid eroded slopes. *Earth Surface Processes and Landforms: The Journal of the British Geomorphological Research Group*, 34(13):1758–1771, 2009.

C. A. Bonilla and O. I. Johnson. Soil erodibility mapping and its correlation with soil properties in central chile. *Geoderma*, 189:116–123, 2012.

P. Borrelli, C. Alewell, P. Alvarez, J. A. A. Anache, J. Baartman, C. Ballabio, N. Bezak, M. Biddoccu, A. Cerdà, D. Chalise, et al. Soil erosion modelling: A global review and statistical analysis. *Science of the total environment*, 780:146494, 2021.

D. D. Breshears, J. J. Whicker, M. P. Johansen, and J. E. Pinder. Wind and water erosion and transport in semi-arid shrubland, grassland and forest ecosystems: Quantifying dominance of horizontal wind-driven transport. *Earth Surface Processes and Landforms: The Journal of the British Geomorphological Research Group*, 28(11):1189–1209, 2003.

B. N. Burnett, G. A. Meyer, and L. D. McFadden. Aspect-related microclimatic influences on slope forms and processes, northeastern arizona. *Journal of Geophysical Research: Earth Surface*, 113 (F3), 2008.

V. T. Chow, D. R. Maidment, and L. W. Mays. Applied hydrology. McGraw-Hill new york, computational experiments. *Proc R Soc London A*, 457:157–189, 2005.

G. Comair, D. McKinney, and D. Siegel. Hydrology of the jordan river basin: Watershed delineation, precipitation and evapotranspiration. *Water Resources Management*, 26(14):4281–4293, 2012.

R. Cronshey. *Urban hydrology for small watersheds*. Number 55. US Department of Agriculture, Soil Conservation Service, Engineering Division, 1986.

J. De Vente and J. Poesen. Predicting soil erosion and sediment yield at the basin scale: scale issues and semi-quantitative models. *Earth-science reviews*, 71(1-2):95–125, 2005.

J. De Vente, J. Poesen, G. Verstraeten, G. Govers, M. Vanmaercke, A. Van Rompaey, M. Arabkhedri, and C. Boix-Fayos. Predicting soil erosion and sediment yield at regional scales: where do we stand? *Earth-Science Reviews*, 127:16–29, 2013.

P. Desmet, J. Poesen, G. Govers, and K. Vandaele. Importance of slope gradient and contributing area for optimal prediction of the initiation and trajectory of ephemeral gullies. *Catena*, 37(3-4): 377–392, 1999.

H. E. Dregne and N.-T. Chou. Global desertification dimensions and costs. *Degradation and restoration of arid lands*, 1:73–92, 1992.

ESA-Worldcover, 2020. URL https://esa-worldcover.org/en.

Esri-Inc. Arcgis pro (version 2.8.3), 2021. URL https://www.esri.com/en-us/arcgis/products/arcgis-pro/overview.

Y. Farhan, D. Zregat, I. Farhan, et al. Spatial estimation of soil erosion risk using rusle approach, rs, and gis techniques: a case study of kufranja watershed, northern jordan. *Journal of Water Resource and Protection*, 5(12):1247, 2013.

Y. Farhan, D. Zreqat, and S. Nawaysa. Assessing the influence of physical factors on spatial soil erosion risk in northern jordan. *Journal of American Science*, 10(7), 2014.

Y. Farhan, O. Anaba, et al. Flash flood risk estimation of wadi yutum (southern jordan) watershed using gis based morphometric analysis and remote sensing techniques. *Open Journal of Modern Hydrology*, 6(02):79, 2016.

M. Felegari, A. Talebi, M. T. Dastorani, and A. S. Rangavar. Efficiency assessment of rangeland hydrology and erosion model (RHEM) for water erosion quantification (case study: Sangane watershed-iran). *Environmental Resources Research*, 2(2):134–146, 2014.

D. Flanagan and M. Nearing. Usda-water erosion prediction project: Hillslope profile and watershed model documentation. *Nserl Rep*, 10:1–123, 1995.

Food, A. O. of the United Nations, Food, A. Organization, U. N. E. Programme, Unesco, and G. E. M. System. *A Provisional Methodology for Soil Degradation Assessment*. Number v. 1. FAO, 1979. ISBN 9789251008690. URL https://books.google.nl/books?id=XyGDQgAACAAJ.

Garmin-Support. GPS accuracy, 2022. URL https://support.garmin.com/en-US/?faq=aZc8RezeAb9LjCDpJplTY7.

E. M. Ghazal and H. I. Yasin. Infiltration and some physical properties of soil. *Al-Rafidain Engineering Journal (AREJ)*, 26(2):250–259, 2021.

D. Goodrich, I. Burns, C. Unkrich, D. J. Semmens, D. Guertin, M. Hernandez, S. Yatheendradas, J. R. Kennedy, and L. R. Levick. Kineros2/agwa: Model use, calibration, and validation. *Transactions of the ASABE*, 55(4):1561–1574, 2012.

G. Govers. Misapplications and misconceptions of erosion models. *Handbook of erosion modelling*, 1:117–134, 2011.

W. H. Green and G. Ampt. Studies on soil phyics. *The Journal of Agricultural Science*, 4(1):1–24, 1911.

M. Haddad, M. Rahbeh, S. Strohmeier, and F. M. Ziadat. Climate change impacts on surface water availability & management of jordan's zarqa river basin using soil and water assessment tool (swat). 2017.

M. E. Haddad, S. M. Strohmeier, K. Nouwakpo, M. Weltz, and G. Sterk. Rangeland restoration in jordan: restoring vegetation cover by water harvesting measures. 2022.

C. He. Integration of geographic information systems and simulation model for watershed management. *Environmental Modelling & Software*, 18(8-9):809–813, 2003.

M. Hernandez, M. A. Nearing, O. Z. Al-Hamdan, F. B. Pierson, G. Armendariz, M. A. Weltz, K. E. Spaeth, C. J. Williams, S. K. Nouwakpo, D. C. Goodrich, et al. The rangeland hydrology and erosion model: A dynamic approach for predicting soil loss on rangelands. *Water Resources Research*, 53(11):9368–9391, 2017.

J. E. Herrick. Monitoring manual for grassland, shrubland and savanna ecosystems. 2005.

M. Huang, J. Gallichand, C. Dong, Z. Wang, and M. Shao. Use of soil moisture data and curve number method for estimating runoff in the loess plateau of china. *Hydrological Processes: An International Journal*, 21(11):1471–1481, 2007.

G. Huluka and R. Miller. Particle size determination by hydrometer method. *Southern Cooperative Series Bulletin*, 419:180–184, 2014.

R. İlay and Y. Kavdir. Impact of land cover types on soil aggregate stability and erodibility. *Environmental monitoring and assessment*, 190(9):1–14, 2018.

ISRIC. Soilgrids, 2017. URL `https://files.isric.org/soilgrids/former/2017-03-10/data`.

B. Jabri and M. A. Hessane. Production of a curve number map using gis techniques in the watershed of the high sebou (morocco). In *E3S Web of Conferences*, volume 150, page 03003. EDP Sciences, 2020.

S. Jomaa, D. A. Barry, A. Brovelli, B. Heng, G. C. Sander, J.-Y. Parlange, and C. W. Rose. Rain splash soil erosion estimation in the presence of rock fragments. *Catena*, 92:38–48, 2012.

S. Khresat. Soil erosion and land degradation in the highlands of jordan. In *EGU General Assembly Conference Abstracts*, pages U2013–U2171. 2013.

R. Lal et al. *Soil erosion research methods*. CRC Press, 1994.

Z.-w. Li, G.-h. Zhang, R. Geng, and H. Wang. Rill erodibility as influenced by soil and land use in a small watershed of the loess plateau, china. *biosystems engineering*, 129:248–257, 2015.

H. Lu, C. J. Moran, and I. P. Prosser. Modelling sediment delivery ratio over the murray darling basin. *Environmental Modelling & Software*, 21(9):1297–1308, 2006.

C. Meyer. General description of the cligen model and its history. *USDA-ARS National Soil Erosion Laboratory: West Lafayette, IN*, 2011.

S. N. Miller, D. J. Semmens, D. C. Goodrich, M. Hernandez, R. C. Miller, W. G. Kepner, and D. P. Guertin. The automated geospatial watershed assessment tool. *Environmental Modelling Software*, 22(3):365–377, 2007. ISSN 1364-8152. doi: https://doi.org/10.1016/j.envsoft.2005.12.004. URL `https://www.sciencedirect.com/science/article/pii/S136481520600003X`. Special section: Advanced Technology for Environmental Modelling.

R. P. C. Morgan. *Soil erosion and conservation*. John Wiley & Sons, 2009.

M. Mosbahi, S. Benabdallah, and M. R. Boussema. Assessment of soil erosion risk using swat model. *Arabian Journal of Geosciences*, 6(10):4011–4019, 2013.

M. Nearing, H. Wei, J. Stone, F. Pierson, K. Spaeth, M. Weltz, D. Flanagan, and M. Hernandez. A rangeland hydrology and erosion model. *Transactions of the ASABE*, 54(3):901–908, 2011.

NOAA. Noaa online weather data (nowdata): Interactive data query system, 2006. URL `https://www.ncei.noaa.gov/access/search/data-search/global-summary-of-the-day?stations=40255099999&dataTypes=MIN&bbox=34.431%2C33.654%2C30.431%2C37.654&startDate=1980-01-01T00%3A00%3A00&endDate=2020-05-31T23%3A59%3A59&pageNum=5`.

S. K. Nouwakpo. Creating a gds file for rhem. March 2022a.

S. K. Nouwakpo. Format editing of cligen storm file for rhem. March 2022b.

J. Nyssen, J. Poesen, J. Moeyersons, E. Luyten, M. Veyret-Picot, J. Deckers, M. Haile, and G. Govers. Impact of road building on gully erosion risk: a case study from the northern ethiopian highlands. *Earth Surface Processes and Landforms: The Journal of the British Geomorphological Research Group*, 27(12):1267–1283, 2002.

T. Oweis and A. Taimeh. Evaluation of a small basin water-harvesting system in the arid region of jordan. *Water resources management*, 10(1):21–34, 1996.

R. Pérez-Rodríguez, M. J. Marques, and R. Bienes. Spatial variability of the soil erodibility parameters and their relation with the soil map at subgroup level. *Science of the Total Environment*, 378(1-2):166–173, 2007.

R. Prăvălie. Drylands extent and environmental issues. a global approach. *Earth-Science Reviews*, 161:259–278, 2016.

S. Ravi, D. D. Breshears, T. E. Huxman, and P. D'Odorico. Land degradation in drylands: interactions among hydrologic–aeolian erosion and vegetation dynamics. *Geomorphology*, 116(3-4): 236–245, 2010.

Z. Rawajfih, D. Daud, and H. Shadfan. Soils of the jordan valley: I. general soil characteristics. *Dirasat (Jordan)*, 1987.

G. Richter and J. F. Negendank. Soil erosion processes and their measurement in the german area of the moselle river. *Earth Surface Processes*, 2(2-3):261–278, 1977.

P. Romero, G. Castro, J. Gómez, and E. Fereres. Curve number values for olive orchards under different soil management. *Soil Science Society of America Journal*, 71(6):1758–1769, 2007.

C. Ross, L. Prihodko, J. Anchang, S. Kumar, W. Ji, and N. Hanan. Global hydrologic soil groups (hysogs250m) for curve number-based runoff modeling, 2018. URL `https://daac.ornl.gov/cgi-bin/dsviewer.pl?ds_id=1566`.

L. Salazar et al. Irrigation training manual. planning, design, operation, and management of small-scale irrigation systems [and] irrigation reference manual. a technical reference to be used with the peace corps irrigation training manual t0076 in the selection, planning, design, operation, and management of small-scale irrigation systems. 1994.

C. Santhi, R. Srinivasan, J. G. Arnold, and J. Williams. A modeling approach to evaluate the impacts of water quality management plans implemented in a watershed in texas. *Environmental modelling & software*, 21(8):1141–1157, 2006.

Z. Sen. *Wadi hydrology*. Crc Press, 2008.

S. Senanayake, B. Pradhan, A. Huete, and J. Brennan. A review on assessing and mapping soil erosion hazard using geo-informatics technology for farming system management. *Remote Sensing*, 12(24):4063, 2020.

H. Sensoy and Ö. Kara. Slope shape effect on runoff and soil erosion under natural rainfall conditions. *iForest-Biogeosciences and Forestry*, 7(2):110, 2014.

M. W. Shammout, M. Shatanawi, and J. Nelson. Curve number applications for restoration the zarqa river basin. *Sustainability*, 10(3):586, 2018.

M. A. Shirazi and L. Boersma. A unifying quantitative analysis of soil texture. *Soil Science Society of America Journal*, 48(1):142–147, 1984.

SIDA-FAO. Project title: 'planning and piloting watershed rehabilitation for improved water productivity with water-harvesting in jordan.'. *An ICARDA project funded by SIDA and FAO.* URL `https://mel.cgiar.org/projects/1621`.

J. Sitterson, C. Knightes, R. Parmar, K. Wolfe, B. Avant, and M. Muche. An overview of rainfall-runoff model types. 2018.

R. E. Smith and J.-Y. Parlange. A parameter-efficient hydrologic infiltration model. *Water Resour. Res.*, 14(3):533–538, June 1978.

StatisticsSolutions. Correlation (pearson, kendall, spearman), Aug 2021. URL `https://www.statisticssolutions.com/free-resources/directory-of-statistical-analyses/correlation-pearson-kendall-spearman/`.

Statology. The five assumptions for pearson correlation, Nov 2021. URL `https://www.statology.org/pearson-correlation-assumptions/`.

S. Strohmeier. *Restoring Degraded Rangelands in Jordan: Optimizing Mechanized Micro Water Harvesting using Rangeland Hydrology and Erosion Model (RHEM). 1st World Conference on Soil and Water Conservation under Global Change-CONSOWAAt.* Lleida, Spain, 2017.

S. Strohmeier, S. Fukai, M. Haddad, M. AlNsour, M. Mudabber, K. Akimoto, S. Yamamoto, S. Evett, and T. Oweis. Rehabilitation of degraded rangelands in jordan: The effects of mechanized micro water harvesting on hill-slope scale soil water and vegetation dynamics. *J. Arid Environ.*, 185(104338):104338, Feb. 2021.

L. Tamene, Z. Adimassu, J. Ellison, T. Yaekob, K. Woldearegay, K. Mekonnen, P. Thorne, and Q. B. Le. Mapping soil erosion hotspots and assessing the potential impacts of land management practices in the highlands of ethiopia. *Geomorphology*, 292:153–163, 2017.

S. J. Thien. A flow diagram for teaching texture-by-feel analysis. *Journal of Agronomic education*, 8(1):54–55, 1979.

UN. Water harvesting for al-mashare' jordan in jordan, feb 2021. URL `https://jordan.un.org/en/110464-water-harvesting-al-mashare-jordan`.

S. USDA. Urban hydrology for small watersheds. *Technical release*, 55:2–6, 1986.

Vallerani-System. Vallerani system srl. 2022. URL `https://www.vallerani.com/wp/wp-content/uploads/2019/05/ENG-tractor_Delfino-3s.pdf`. Accessed: 2022-5-26.

K. Vandaele, J. Poesen, G. Govers, and B. van Wesemael. Geomorphic threshold conditions for ephemeral gully incision. *Geomorphology*, 16(2):161–173, 1996.

J.-P. Venot, F. Molle, and R. Courcier. Dealing with closed basins: The case of the lower jordan river basin. *Int. J. Water Resour. Dev.*, 24(2):247–263, June 2008.

S. Veron, J. Paruelo, and M. Oesterheld. Assessing desertification. *Journal of Arid Environments*, 66(4):751–763, 2006.

B. Wang, F. Zheng, M. J. Römkens, and F. Darboux. Soil erodibility for water erosion: A perspective and chinese experiences. *Geomorphology*, 187:1–10, 2013.

H. Wang, G.-h. Zhang, N.-n. Li, B.-j. Zhang, and H.-y. Yang. Variation in soil erodibility under five typical land uses in a small watershed on the loess plateau, china. *Catena*, 174:24–35, 2019.

H. Wheater and R. Al Weshah. Hydrology of wadi systems. 2002.

D. A. Woolhiser, R. E. Smith, D. C. Goodrich, et al. Kineros: a kinematic runoff and erosion model: documentation and user manual. 1990.

WorldBank. World bank climate change knowledge portal, 2021. URL `https://climateknowledgeportal.worldbank.org/country/jordan/climate-data-historical`.

A. Yair. Water-harvesting efficiency in arid and semiarid areas. In *Sustainable Land Use in Deserts*, pages 289–302. Springer, 2001.

L. Yaoming, Z. Qiang, and C. Deliang. Stochastic modeling of daily precipitation in china. *Journal of Geographical Sciences*, 14(4):417–426, 2004.

M. Yibeltal, A. Tsunekawa, N. Haregeweyn, E. Adgo, D. T. Meshesha, T. Masunaga, M. Tsubo, P. Billi, K. Ebabu, A. A. Fenta, et al. Morphological characteristics and topographic thresholds of gullies in different agro-ecological environments. *Geomorphology*, 341:15–27, 2019.

R. Zhang, X. Liu, G. C. Heathman, X. Yao, X. Hu, and G. Zhang. Assessment of soil erosion sensitivity and analysis of sensitivity factors in the Tongbai–Dabie mountainous area of china. *Catena*, 101:92–98, Feb. 2013.

F. M. Ziadat and A. Taimeh. Effect of rainfall intensity, slope, land use and antecedent soil moisture on soil erosion in an arid environment. *Land Degradation & Development*, 24(6):582–590, 2013.

Appendix A

RHEM main equations

Corresponding descriptions of the equations below can be retrieved from (Hernandez et al., 2017).

Overland Flow Equations in RHEM V2.3:

(1)
$$\frac{\partial h}{\partial t} + \frac{\partial q}{\partial x} = \sigma(x,t)$$

(2)
$$\sigma(x,t) = r - f$$

(3)
$$q = \left(\frac{8gS}{f_t}\right)^{1/2} h^{3/2}$$

(4)
$$\frac{\partial h}{\partial t} + \frac{3}{2}\left(\frac{8gS}{f_t}\right)^{1/2} h^{1/2}\frac{\partial h}{\partial x} = r - f$$

(5)
$$h(0,t) = 0$$

(6)
$$f = K_e\left[1 + \frac{\propto}{\exp\left(\frac{\alpha l}{C_d \Delta\theta_i}\right) - 1}\right]$$

Overland Soil Erosion, Deposition, and Transport Equations in RHEM V2.3:

(7)
$$\frac{\partial (Ch)}{\partial t} + \frac{\partial \left(Cq_r\right)}{\partial x} = D_{ss} + D_{cf}$$

(8)
$$q_r = \frac{q}{w}$$

(9)
$$w = \frac{2.46Q^{0.39}}{S^{0.4}}$$

(10)
$$D_{ss} = K_{ss} r^{1.052} \sigma^{0.592}$$

(11)
$$D_{cf} = \left[\begin{array}{l} D_c \left(1 - \frac{CQ}{T_c}\right), CQ \leq T_c \\ \frac{0.5V_f}{Q} \left(T_c - CQ\right), CQ \geq T_c \end{array} \right]$$

(12)
$$D_c = K_\omega(\omega)$$

(13)
$$\log_{10}\left(\frac{10T_c}{w}\right) = -34.47 + 38.61 * \frac{\exp[0.845 + 0.412\log(1000\omega)]}{1 + \exp[0.845 + 0.412\log(1000\omega)]}$$

(14)
$$D_c = K_{\omega(Max)adj} \exp\left(\beta q_c\right) \omega$$

(15)
$$q_c = \int q_r dt$$

(16)
$$\omega = \gamma S q_r$$

Appendix B

Python scripts

B.1 Create GDS file

Nouwakpo (2022a)

```
import os
import datetime as dt


def complete_to_max(string_to_expand):
    out_string = '{:^46}'.format(string_to_expand)
    return out_string


name = "Kufr Awan station"

latitude = '{degree:3d}{minutes:2d}'.format(degree=32, minutes=43)
longitude = '{degree:3d}{minutes:2d}'.format(degree=360-35, minutes=69)
elevation = '{:6d}'.format(470)

header = "40250"+complete_to_max(name)+latitude+"  "+longitude+elevation+"\n"
fhout = open('JordanSite.GDS', 'w')
fhout.write(header)
##The input file name is JordanSite.txt
##And we want to output the JordanSite.GDS
fhin = open('JordanSite.txt', 'r')
#Reads header
fhin.readline()
for line in fhin:
    line = line.strip('\n')
    line = line.strip('\r')
    arr = line.split('\t')
    if line:
        date_ = dt.datetime.strptime(arr[0], "%m/%d/%Y")
        if arr[4] != '':
            maxT = '{:5.0f}'.format(float(arr[4])*10)
        else:
            maxT = '{:5.0f}'.format(-999)
        if arr[5] != '':
            minT = '{:5.0f}'.format(float(arr[5])*10)
```

```
        else:
            minT = '{:5.0f}'.format(-999)
        if arr[6] != '':
            P = '{:5.0f}'.format(float(arr[6])*10)
        else:
            P = '{:5.0f}'.format(-999)

        fhout.write('%s%s  %s  %s\n'%(date_.strftime("%y%m%d"), maxT, minT, P))
fhout.close()
fhin.close()
```

B.2 Re-format storm file

Nouwakpo (2022b)

```
import os
import re
import io


def format_file(fname):
    fh = open(fname, 'r')
    pref, ext = os.path.splitext(fname)
    #print ext
    new_name = "%s_ref%s"%(pref, ext)

    fh2 = open(new_name, 'w')
    line = ''
    while "da mo year  prcp" not in line:
        refline = "# %s"%line
        fh2.write(refline)
        line = fh.readline()
    temp_ = io.StringIO()
    if "da mo year  prcp" in line:
        refline = "%s%s%s%s%s%s%s%s%s\n"%('#'.ljust(1),\
                                          'id'.rjust(8),\
                                         'day'.rjust(8),\
                                         'month'.rjust(8),\
                                         'year'.rjust(8),\
                                         'Rain'.rjust(8),
                                         'Dur'.rjust(8),\
                                         'Tp'.rjust(8),\
                                         'Ip'.rjust(8))

        temp_.write(refline)

        refline = "%s%s%s%s%s%s%s%s%s\n"%('#'.ljust(1),\
                                          ' '.rjust(8),\
                                         ' '.rjust(8),\
                                         ' '.rjust(8),\
                                         ' '.rjust(8),\
                                         '(mm)'.rjust(8),
                                         '(h)'.rjust(8),\
                                         ' '.rjust(8),\
                                         ' '.rjust(8))
        temp_.write(refline)
```

```
    fh.readline()
    cnt = 0

    for line in fh:
        line = re.sub(' +', ' ', line)
        line = line.strip('\n')
        line = line.strip('\r')
        arr = line.split(' ')
        if len(arr) < 8:
            continue
        if float(arr[4]) <= 0.0:
            continue
        else:
            cnt+=1
            refline = "%s%s%s%s%s%s%s%s%s\n"%(' '.rjust(1),\
                                              str(cnt).rjust(8),\
                                              arr[1].rjust(8),\
                                              arr[2].rjust(8),\
                                              arr[3].rjust(8),\
                                              arr[4].rjust(8),
                                              arr[5].rjust(8),\
                                              arr[6].rjust(8),\
                                              arr[7].rjust(8))
            temp_.write(refline)
    fh.close()
    fh2.write("%i # The number of rain events\n"%cnt)
    fh2.write("0 # Breakpoint data? (0 for no, 1 for yes)\n")
    fh2.write(temp_.getvalue())
    fh2.close()

## JordanSite.CLI is our input file name (output of the cligen run)
## The output would be JordanSite_ref.CLI
## The CLI extension is arbitrary, it could be .out or any extension we desire
format_file('JordanSite.CLI')
```

B.3 RCC and SCC estimation

```
import pandas as pd
import copy
import numpy as np
from datetime import timedelta


#importing and creating copy of DataFrame
df = pd.read_csv('D3-20B_python.csv', sep=';', decimal=",", parse_dates=['Date'],
    dayfirst=True)
df = copy.deepcopy(df)

#cleaning data
df = df[['Date','ID', 'Day', 'Month', 'Year', 'Q_runoff', 'soil_loss']]

#function that calculates runoff- and soil capturing capacity (RCC and SCC) per
    plotsize based on
#depth of pit, infiltration rate and the trapping efficiency (TE) equation.
def RCC_SCC(depth, infil, a, b, c):

```

```
    #setting initial water level in pit at 0 mm
    level = 0
    #empty list to store water level in pit per day in mm
    list_level = []
    #empty list to store superfluous levels per day in mm
    list_remaining = []
    #calculation of next day
    next_day = df['Date'].iloc[0]
    #loop for every event
    for ID, row in df.iterrows():
        if row['Date'] == next_day:
            #add runoff in mm to level in pit
            level += row['Q_runoff']
            #calculate superfluous levels
            remaining = level - depth
            #if superfluous levels are negative, set to zero.
            if remaining < 0:
                remaining = 0
            #if max depth is attained and superfluous levels occur, set level to max
    .
            elif remaining > 0:
                level = depth
            #add current level for that day to corresponding list
            list_level.append(level)
            #add superfluous level for that day to corresponding list
            list_remaining.append(remaining)
            #substract the infiltration rate for the beginning of the next event
            level -= infil
            #check if level is negative, if so, make it 0.
            if level < 0:
                level = 0
            #make new next day
            next_day = row['Date'] + timedelta(days=1)
        else:
            #substract extra infiltration for the beginning of the event(so double
    infil)
            level -= infil
            #check if level is negative, if so, make it 0.
            if level < 0:
                level = 0
            #add runoff in mm to level in pit
            level += row['Q_runoff']
            #calculate superfluous levels
            remaining = level - depth
            #if superfluous levels are negative, set to zero.
            if remaining < 0:
                remaining = 0
            #if max depth is attained and superfluous levels occur, set level to max
    .
            elif remaining > 0:
                level = depth
            #add current level for that day to corresponding list
            list_level.append(level)
            #add superfluous level for that day to corresponding list
            list_remaining.append(remaining)
            #substract the infiltration rate for the beginning of the next event
            level -= infil
            #check if level is negative, if so, make it 0.
```

```
            if level < 0:
                level = 0
            #make new next day
            next_day = row['Date'] + timedelta(days=1)

    #add created lists to data frame
    df['Pit level'] =  np.array(list_level)
    df['Excess'] =  np.array(list_remaining)

    #creating average TE list
    list_te = []

    #loop for every event (POLYNOMIAL TE function)
    for ID, row in df.iterrows():
        trapping_efficiency = (a * (row['Excess']**2))-(b * row['Excess']) + c
        list_te.append(trapping_efficiency)

    #add lists to data frame
    df['trap_eff'] = np.array(list_te)

    #add sediment capture to data frame
    df['sed_cap'] = df["soil_loss"] * df["trap_eff"]

    #save dataframe to excel spreadsheet(in same folder as running code from)
    df.to_excel('df.xlsx', index = False)

    #print decreased runoff in percentage to console
    print(f"The surface runoff decreased by {abs(round((df['Excess'].sum() - df['
    Q_runoff'].sum()) / df['Q_runoff'].sum() * 100, 2))} percent.")

    #print decreased soil loss in percentage to console
    print(f"The soil loss decreased by {abs(round((df['sed_cap'].sum()) / df['
    soil_loss'].sum() * 100, 2))} percent.")

#running the function (depth, infil, a, b, c)
RCC_SCC(5, 4.5, 0.0002, 0.0255, 0.9893)
```

Appendix C

Relation rainfall- and runoff station

The figures below show the relationship between rainfall station Kufr Awan (ID: AB0008) and runoff station Wadi Ziglab (ID: AF0003).

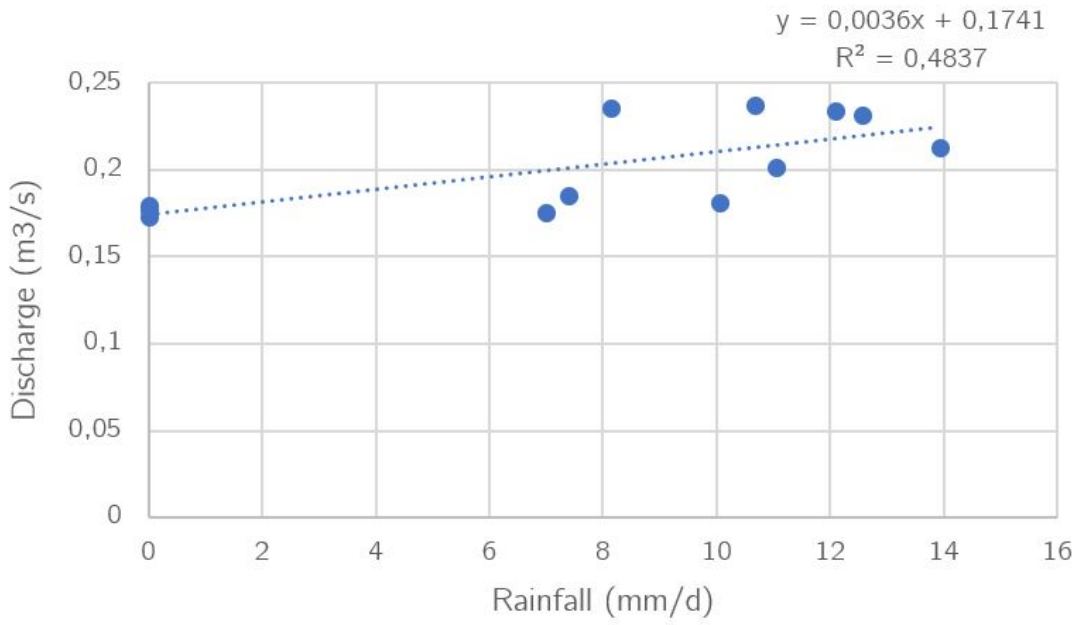

Figure C.1: Average monthly rainfall vs discharge (1980-2018)

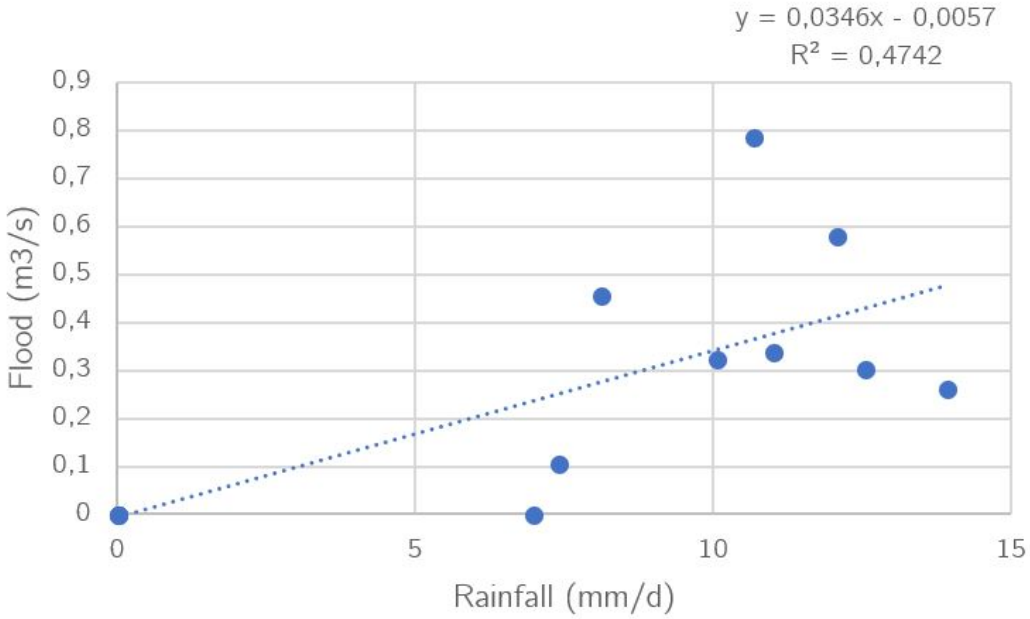

Figure C.2: Average monthly rainfall vs flood (1980-2018)

Appendix D

ESA Worldcover class definitions

Coding of the ESA-Worldcover (2020) map and definition of the classes:

Map code	Land Cover Class	LCCS code	Definition	Color code (RGB)
10	Tree cover	A12A3 // A11A1 A24A3C1(C2)-R1(R2)	This class includes any geographic area dominated by trees with a cover of 10% or more. Other land cover classes (shrubs and/or herbs in the understorey, built-up, permanent water bodies, ...) can be present below the canopy, even with a density higher than trees. Areas planted with trees for afforestation purposes and plantations (e.g. oil palm, olive trees) are included in this class. This class also includes tree covered areas seasonally or permanently flooded with fresh water except for mangroves.	0,100,0
20	Shrubland	A12A4 // A11A2	This class includes any geographic area dominated by natural shrubs having a cover of 10% or more. Shrubs are defined as woody perennial plants with persistent and woody stems and without any defined main stem being less than 5 m tall. Trees can be present in scattered form if their cover is less than 10%. Herbaceous plants can also be present at any density. The shrub foliage can be either evergreen or deciduous.	255, 187, 34
30	Grassland	A12A2	This class includes any geographic area dominated by natural herbaceous plants (Plants without persistent stem or shoots above ground and lacking definite firm structure): (grasslands, prairies, steppes, savannahs, pastures) with a cover of 10% or more, irrespective of different human and/or animal activities, such as: grazing, selective fire management etc. Woody plants (trees and/or shrubs) can be present assuming their cover is less than 10%. It may also contain uncultivated cropland areas (without harvest/ bare soil period) in the reference year	255, 255, 76
40	Cropland	A11A3(A4)(A5) // A23	Land covered with annual cropland that is sowed/planted and harvestable at least once within the 12 months after the sowing/planting date. The annual cropland produces an herbaceous cover and is sometimes combined with some tree or woody vegetation. Note that perennial woody crops will be classified as the appropriate tree cover or shrub land cover type. Greenhouses are considered as built-up.	240, 150, 255
50	Built-up	B15A1	Land covered by buildings, roads and other man-made structures such as railroads. Buildings include both residential and industrial building. Urban green (parks, sport facilities) is not included in this class. Waste dump deposits and extraction sites are considered as bare.	250, 0, 0
60	Bare / sparse vegetation	B16A1(A2) // B15A2	Lands with exposed soil, sand, or rocks and never has more than 10 % vegetated cover during any time of the year	180, 180, 180
70	Snow and Ice	B28A2(A3)	This class includes any geographic area covered by snow or glaciers persistently	240, 240, 240
80	Permanent water bodies	B28A1(B1) // B27A1(B1)	This class includes any geographic area covered for most of the year (more than 9 months) by water bodies: lakes, reservoirs, and rivers. Can be either fresh or salt-water bodies. In some cases the water can be frozen for part of the year (less than 9 months).	0, 100, 200
90	Herbaceous wetland	A24A2	Land dominated by natural herbaceous vegetation (cover of 10% or more) that is permanently or regularly flooded by fresh, brackish or salt water. It excludes unvegetated sediment (see 60), swamp forests (classified as tree cover) and mangroves see 95)	0, 150, 160
95	Mangroves	A24A3C5-R3	Taxonomically diverse, salt-tolerant tree and other plant species which thrive in intertidal zones of sheltered tropical shores, "overwash" islands, and estuaries.	0, 207, 117
100	Moss and lichen	A12A7	Land covered with lichens and/or mosses. Lichens are composite organisms formed from the symbiotic association of fungi and algae. Mosses contain photo-autotrophic land plants without true leaves, stems, roots but with leaf-and stemlike organs.	250, 230, 160

Appendix E

Flow diagram texture feel analysis

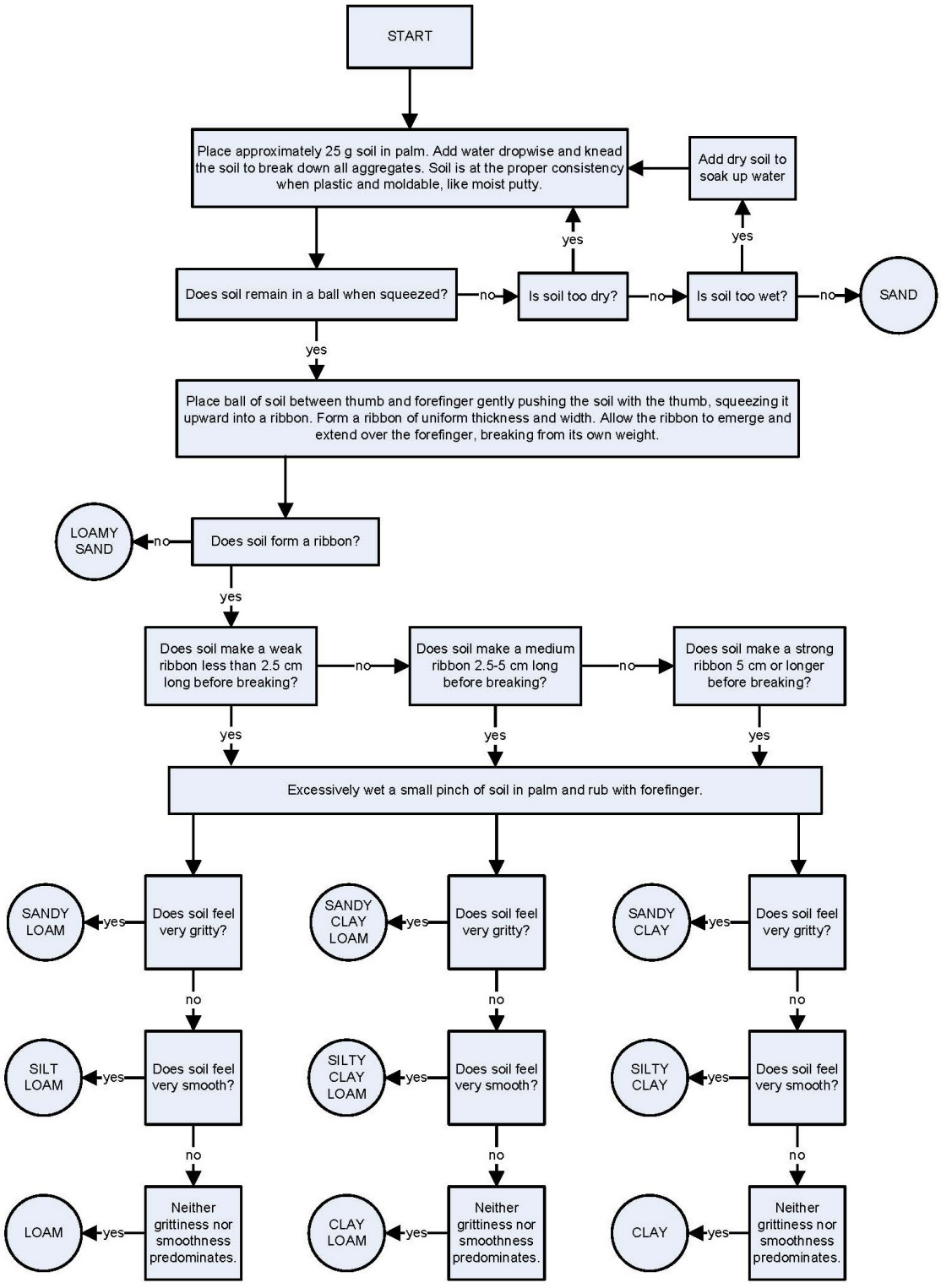

Figure E.1: Adopted from Thien (1979)

Appendix F

Line-point intercept template

Line-point Intercept Data Form

Page _____ of _____ **Shaded cells for calculations**

Plot: _____ Line #: _____ Observer: _____ Recorder: _____

Direction: _____ Date: _____ Intercept (Point) Spacing Interval = _____ cm (___ in)

Pt.	Top layer	Lower layers Code 1	Code 2	Code 3	Soil surface	Pt.	Top layer	Lower layers Code 1	Code 2	Code 3	Soil surface
1						26					
2						27					
3						28					
4						29					
5						30					
6						31					
7						32					
8						33					
9						34					
10						35					
11						36					
12						37					
13						38					
14						39					
15						40					
16						41					
17						42					
18						43					
19						44					
20						45					
21						46					
22						47					
23						48					
24						49					
25						50					

% foliar cover = ____ top layer pts (1st col) x 2 = ____ %

% bare ground* = ____ pts (w/NONE over S) x 2 = ____ %

% basal cover = ____ plant base pts (last col) x 2 = ____ %

Top layer codes: Species code, common name, or NONE (no cover).

Lower layers codes: Species code, common name, L (herbaceous litter), WL (woody litter, >5 mm (~1/4 in) diameter).

Unknown Species Codes:

AF# = annual forb
PF# = perennial forb
AG# = annual graminoid
PG# = perennial graminoid
SH# = shrub
TR# = tree

Soil Surface (do not use litter):

Species Code (for basal intercept)

R = rock fragment (>5 mm (~1/4 in) diameter)
BR = bedrock, M = moss
LC = visible biotic crust on soil
S = soil without any other soil surface code
EL = embedded litter (see page 10)
D = duff

**Bare ground occurs ONLY when Top layer = NONE, Lower layers are empty (no L), and Soil surface = S.*

Appendix G

Stream network statistics

Regression statistics of the relation between slope length and steepness:

SUMMARY OUTPUT

Regression Statistics	
Multiple R	0,612954238
R Square	0,375712898
Adjusted R Square	0,358371589
Standard Error	19,98759643
Observations	38

ANOVA

	df	*SS*	*MS*	*F*	*Significance F*
Regression	1	8655,564288	8655,56	21,6658	4,29462E-05
Residual	36	14382,1444	399,504		
Total	37	23037,70868			

	Coefficients	*Standard Error*	*t Stat*	*P-value*	*Lower 95%*	*Upper 95%*	*Lower 95,0%*	*Upper 95,0%*
Intercept	34,0150317	10,89378379	3,12243	0,00353	11,92141414	56,108649	11,9214141	56,10864926
slope ° (y)	3,049484497	0,655147833	4,65465	4,3E-05	1,720783108	4,3781859	1,72078311	4,378185887